Earth-Science Reviews 150 (2015) 724–745

Contents lists available at ScienceDirect

Earth-Science Reviews

journal homepage: www.elsevier.com/locate/earscirev

Antarctic ice rises and rumples: Their properties and significance for ice-sheet dynamics and evolution

Kenichi Matsuoka [a,*], Richard C.A. Hindmarsh [b], Geir Moholdt [a], Michael J. Bentley [c], Hamish D. Pritchard [b], Joel Brown [a,1], Howard Conway [d], Reinhard Drews [e], Gaël Durand [f,g], Daniel Goldberg [h], Tore Hattermann [i,j], Jonathan Kingslake [b], Jan T.M. Lenaerts [k], Carlos Martín [b], Robert Mulvaney [b], Keith W. Nicholls [b], Frank Pattyn [e], Neil Ross [l], Ted Scambos [m], Pippa L. Whitehouse [c]

[a] Norwegian Polar Institute, Framsenteret, Tromsø 9296, Norway
[b] British Antarctic Survey, High Cross, Madingley Road, Cambridge CB3 0ET, UK
[c] Department of Geography, Durham University, Lower Mountjoy, South Road, Durham DH1 3LE, UK
[d] Department of Earth and Space Sciences, University of Washington, Seattle, WA 98195-1310, USA
[e] Laboratoire de Glaciologie, Université Libre de Bruxelles, Avenue F.D. Roosevelt 50, B-1050 Brussels, Belgium
[f] CNRS, LGGE, F-38041 Grenoble, France
[g] University Grenoble Alps, LGGE, F-38041 Grenoble, France
[h] School of Geoscience, University of Edinburgh, Drummond Street, Edinburgh EH8 9XP, UK
[i] Akvaplan-niva AS, Framsenteret, Tromsø 9296, Norway
[j] Alfred Wegener Institute, Helmholtz Centre for Polar and Marine Research, Bremerhaven, Germany
[k] Institute for Marine and Atmospheric Research, Utrecht University, P.O. Box 80005, 3508 TA Utrecht, The Netherlands
[l] School of Geography, Politics, and Sociology, Newcastle University, Newcastle Upon Tyne NE1 7RU, UK
[m] National Snow and Ice Data Center, Cooperative Institute for Research in Environmental Sciences, University of Colorado, Boulder, CO 80309-0449, USA

ARTICLE INFO

Article history:
Received 8 May 2015
Received in revised form 4 September 2015
Accepted 11 September 2015
Available online 15 September 2015

Keywords:
Antarctic Ice Sheet
Holocene deglaciation
Sea-level rise
Pinning point
Ice dome

ABSTRACT

Locally grounded features in ice shelves, called ice rises and rumples, play a key role buttressing discharge from the Antarctic Ice Sheet and regulating its contribution to sea level. Ice rises typically rise several hundreds of meters above the surrounding ice shelf; shelf flow is diverted around them. On the other hand, shelf ice flows across ice rumples, which typically rise only a few tens of meters above the ice shelf. Ice rises contain rich histories of deglaciation and climate that extend back over timescales ranging from a few millennia to beyond the last glacial maximum. Numerical model results have shown that the buttressing effects of ice rises and rumples are significant, but details of processes and how they evolve remain poorly understood. Fundamental information about the conditions and processes that cause transitions between floating ice shelves, ice rises and ice rumples is needed in order to assess their impact on ice-sheet behavior. Targeted high-resolution observational data are needed to evaluate and improve prognostic numerical models and parameterizations of the effects of small-scale pinning points on grounding-zone dynamics.

Contents

* Corresponding author.
E-mail address: matsuoka@npolar.no (K. Matsuoka).
[1] Current affiliation: Aesir Consulting LLC, Missoula, MT, 59081, USA.

http://dx.doi.org/10.1016/j.earscirev.2015.09.004
0012-8252/

1. Introduction

Small-scale topographic features occur wherever ice shelves ground locally on the elevated seabed. These features are called “ice rises” where the flowing ice shelf is diverted around the grounded region, and “ice rumples” where the ice shelf flows over the grounded region (Figs. 1 and 2). Numerous ice rises around the edge of the Antarctic Ice Sheet are in fact miniature ice sheets — independent entities with many of the characteristics shared with the larger, main ice sheet (Robin, 1953). Being smaller and numerous, ice rises represent a far larger sample of possible ice sheets. Each one is relatively simple, but the population provides much variety. As such, they provide a convenient platform for conducting geophysical and glaciological observations and model experiments to develop concepts about ice sheets.

Understanding the role of ice rises in the evolution and future of the Antarctic Ice Sheet is important for three primary reasons. First, glacial-interglacial changes in the extent and configuration of the Antarctic Ice Sheet are largest at the margins, so knowledge from ice rises provide powerful constraints on the timing and amount of thickness changes (e.g., Conway et al., 1999; Brook et al., 2005; Waddington et al., 2005; Martin et al., 2006; Mulvaney et al., 2007). Second, relatively high surface mass balance (SMB) and close proximity to the storm track that circulates Antarctica make ice cores from ice rises well suited to examine highly regional, circumpolar variations in Antarctic climate and sea ice, and their tele-connections (e.g., Goodwin et al., 2014; Sinclair et al., 2014). Finally, the mass balance of Antarctica is dominated by grounding-zone dynamics and ice-shelf/ocean interactions, which are influenced by ice rises and rumples. For example it is thought that recent un-grounding of an ice rumple within the ice shelf of Pine Island Glacier in the Amundsen Sea Embayment has contributed to the ongoing retreat and thinning in the region (Jenkins et al., 2010a; Gladstone et al., 2012). Losses from the Amundsen Sea Embayment dominate the current mass deficit of the Antarctic Ice Sheet (Pritchard et al., 2012; Joughin et al., 2014; Rignot et al., 2014). Ice rumples are much smaller than ice rises, but provide significant buttressing to the ice shelf with potential for rapid ice-dynamical changes in cases of grounding or un-grounding.

Here, we review current understanding of ice rises and rumples in terms of their morphology, distribution, history, and impact on the evolution of Antarctica. Section 2 first defines ice rises and rumples and then shows their distributions, and their geological, oceanographic, and climatological settings. We also discuss their formation mechanisms. Section 3 reviews the roles of ice rises and rumples in ice-sheet dynamics and mass balance. Section 4 provides an overview of current knowledge of the Holocene retreat of the Antarctic Ice Sheet, with emphasis on the records and roles of ice rises. Finally, in Section 5, we discuss major knowledge gaps, and key directions and needs for future research.

2. Settings

2.1. Definition of ice rises and rumples

Ice rises and ice rumples are locally elevated, grounded features surrounded fully or partially by ice shelves or ice streams (Figs. 1 and 2). Other terms such as ice hill, ice dome, ice promontory, ice ridge, and inter-ice-stream ridge have also been used to refer to ice rises (depending on which characteristic is being emphasized), so we include them in our definition here. We follow MacAyeal et al. (1987) to distinguish ice rises and rumples.

Ice rises are built mostly from locally accumulating snow. They consist of radial ice-flow centers or divides separate from the main ice sheet. They are typically several hundred meters higher than the surrounding ice shelves or ice streams. In cross section (Fig. 2), the surface topography is quasi parabolic with flank slopes extending from a blunt peak (Martin and Sanderson, 1980). Local snow accumulation and negligible horizontal ice flow make the flow divide or center an excellent site to extract ice cores to determine coastal Antarctic climate. Examples of ice rises of various types include (see Figs. 1 and 3 for locations): (#1) Roosevelt Island in the Ross Sea Embayment and Korff Ice Rise in the Weddell Sea Embayment are isles completely surrounded by ice shelves; (#2) Fletcher Promontory in the Weddell Sea Embayment is a promontory of the ice sheet protruding into the ice shelf; (#3) Siple Dome in the Ross Sea Embayment is an inter-ice-stream ridge; and

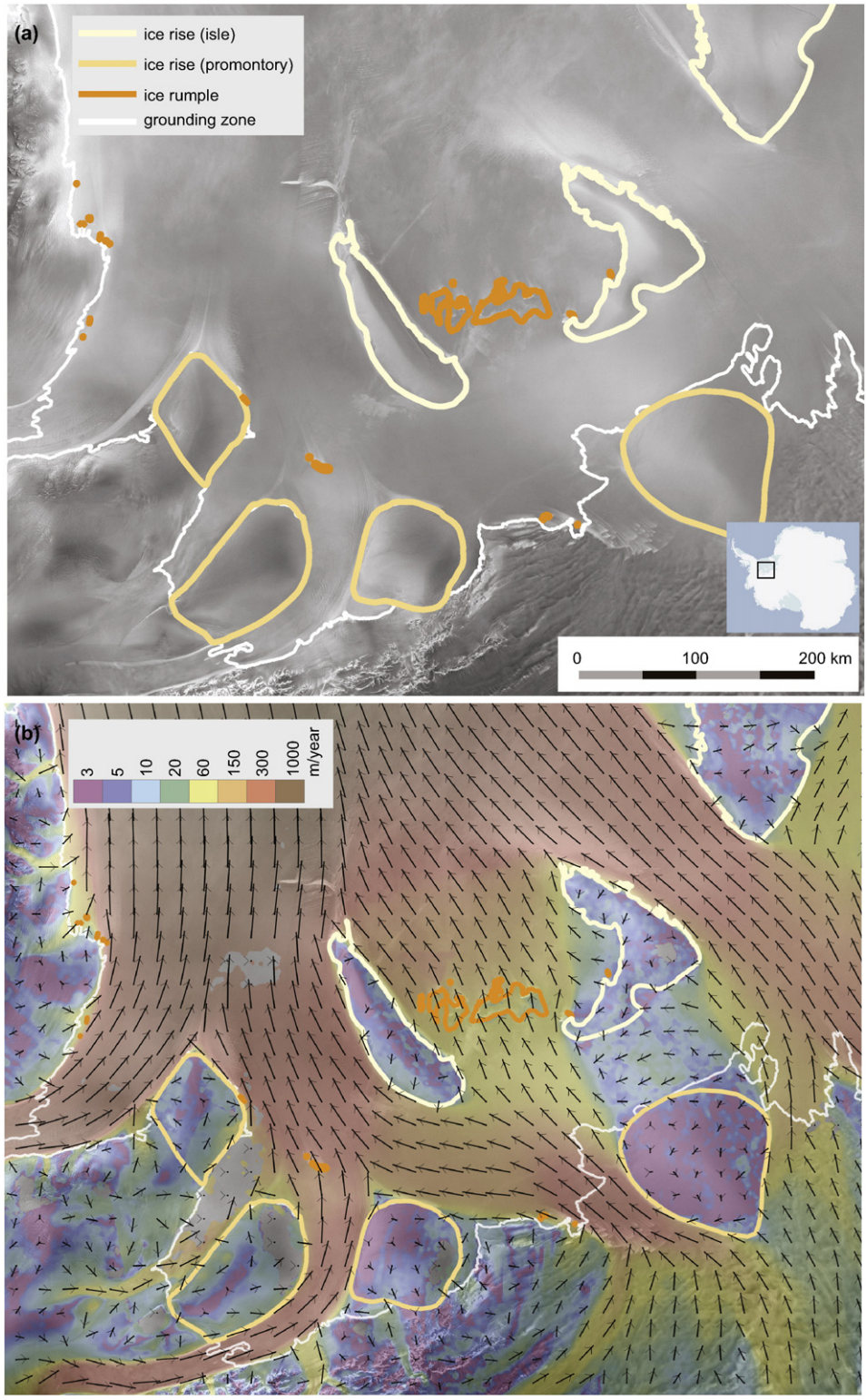

Fig. 1. Ice rises and rumples in the Ronne–Filchner Ice Shelf, West Antarctica. Inset shows the location. Outlined are ice rises and rumples inventoried in this study (see Appendix A). Bed topography in this region and names of these ice rises and rumples are shown in Fig. 6b. The grounding zone of the ice sheet is also shown (Bindschadler et al., 2011). (a) Morphological structures associated with ice rises and rumples visible in Radarsat-2 satellite imagery (Jezek et al., 2002). Brightness changes are associated with surface-slope variations of major ice rises, as well as crevasses and rifts in the ice shelf. (b) Ice flow field (Rignot et al., 2011a) perturbed by ice rises and rumples. Arrow lengths are proportional to the logarithm of ice-flow speeds.

(#4) Dorsey Island in the Wilkins Ice Shelf is an island that consists of both ice and outcrops of bedrock or sediments. Ice rises in categories #2 and #3 are elongate extensions of the inland ice sheet into the ice shelf, but have saddles between the adjacent inland ice sheet and seaward local flow centers at elevations that are higher than the proximal grounded ice sheet.

Ice rumples, on the other hand, are fully enclosed within ice shelves and are typically elevated only tens of meters or less from the ice-shelf

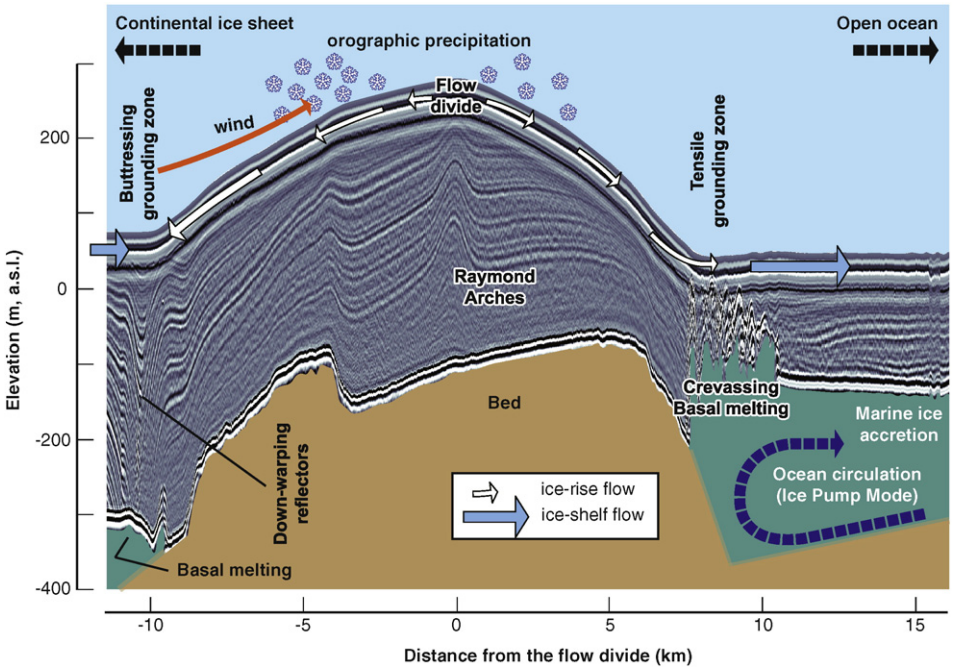

Fig. 2. Cross section of an ice rise. The radargram is from an along-flow, ground-based profile across the summit of Kupol Ciolkovskogo near the Fimbul Ice Shelf, Dronning Maud Land (K. Matsuoka and J. Brown, unpublished data). Dominant wind direction is oblique to the cross section, and seabed beneath the ocean cannot be detected using radar. The sketches of orographic precipitation and seabed are included for illustration purposes.

surface. Some ice rumples exist at the calving front of the ice shelf, partly facing the ocean. Others are located near ice rises or within grounding zones or lightly grounded ice plains (Brunt et al., 2011). Ice flows across rumples and maintains the same general flow direction as that in the adjacent ice shelf (Fig. 1b). Shearing can occur at the base and most of the ice within rumples is not locally accumulated. Examples are Doake

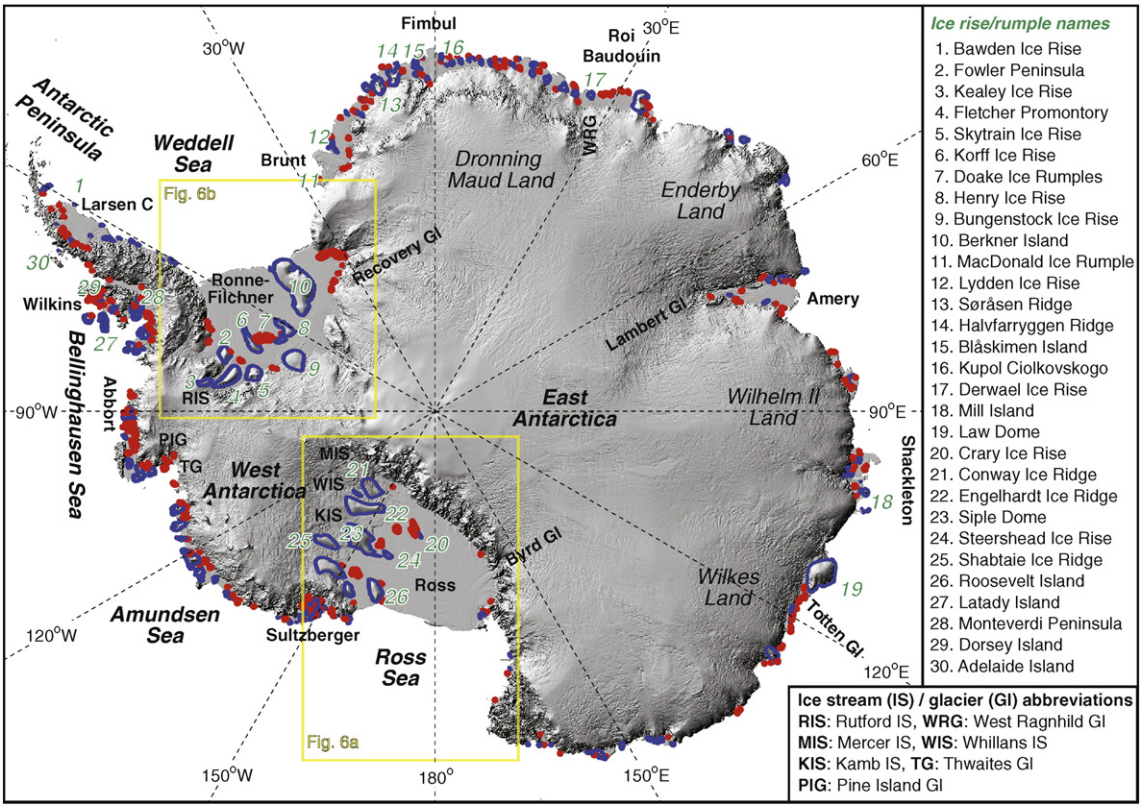

Fig. 3. Locations of ice rises (blue, outlined) and ice rumples (red) in Antarctica, which are included in the inventory (Appendix A). Red markers for ice rumples do not represent their dimensions. The background image is a shaded relief map of the Bedmap2 digital-elevation model (Fretwell et al., 2013). Ice streams, glaciers, and ice shelves mentioned in the text are labeled and major ice rises and rumples are indicated with numbers. Bed topography in the Ross and Weddell Seas are shown in Fig. 6a and b, respectively.

Ice Rumples between Korff and Henry Ice Rises in the central part of the Ronne–Filchner Ice Shelf (Fig. 1). Field observations across ice rumples are sparse (Limbert, 1964; Thomas, 1973b; Swithinbank, 1977; Smith, 1986; Smith, 1991), mainly because the presence of crevasses and rifts hamper surface travel. A notable exception is an ice rumple that was present near the grounding zone of Pine Island Glacier; ice shelf and seabed topography were mapped by an airborne survey and autonomous underwater vehicle (Jenkins et al., 2010a; Jacobs et al., 2011). Here, we do not consider features that ground ephemerally over tidal cycles as ice rumples, because such features provide little buttressing to the ice shelf (Section 3) and their detection using satellite techniques depends on the timing of the observation. Nevertheless, these ephemerally grounded features can readily become ice rumples if the ice shelf thickens or relative sea level lowers.

2.2. Identification by satellite remote sensing

The elevated topography of ice rises and rumples and their ice-flow perturbations in ice shelves such as crevasses and rifts are well imaged by a variety of satellites (Fig. 1a). Visible, near-infrared-band, and microwave imagery, such as that from AVHRR, MODIS, Landsat, ASTER, SPOT, and Radarsat all show brightness changes associated with surface-slope variations in the grounding zone, and also at the crest of ice rises (e.g., Martin, 1976; Scambos et al., 2007). In addition, abrupt elevation variations relative to ice shelves can be detected using high-resolution (~10^2 m) lidar and radar altimeters such as ICESat and CryoSat-2. Further, comparisons of repeat altimetry profiles at different times of the tidal cycle have been used to identify ephemerally grounded features (Fricker and Padman, 2006).

The modulated ice flow of grounded features, such as separate flow centers on ice rises and slower or slightly redirected ice flow over rumples can be detected using interferometric techniques of microwave synthetic aperture radar (SAR) and feature tracking of optical or SAR images (Fig. 1b). SAR interferograms can also reveal variations in tidal flexure associated with the grounding zones, which is particularly useful for identifying small rumples that do not induce shear margins and cannot be visually identified in satellite imagery (e.g., Schmeltz et al., 2001; Rignot, 2002; Scambos et al., 2007). However, delineation of ice-flow centers and divides where surface velocities are small is difficult using ice-flow mapping techniques (e.g., Fig. 1b) and thus the distinction between ice rises and rumples is equivocal. An example of such uncertain characterization is Steershead Ice Rise near Siple Dome in the Ross Sea Embayment (Fig. 3).

2.3. Inventory of ice rises and rumples

The Appendix A contains a satellite-derived inventory of Antarctic ice rises and rumples. The presence of localized ice flow from flow centers or divides is the clearest criterion for distinguishing ice rises from rumples. However, the elevation-based approach described in the Appendix A is a more practical way to classify these features. In total, we inventoried 103 isle-type ice rises (group 1), 67 promontory-type ice rises (group 2, including 9 inter-ice-stream ridges), 510 ice rumples (group 3), and 24 elevated features with outcrops (group 4).

Ice rises and ice rumples exist on every major ice shelf in Antarctica (Fig. 3), but the spatial distribution varies. For example, the Siple Coast has a greater number of relatively large ice rises, whereas the Sulzberger and Abbott Ice Shelves contain many small ice rises and rumples. In contrast, few ice rises and rumples exist near the outlets of major glaciers situated in deep bed troughs (e.g., Byrd Glacier in the Ross Sea Embayment and Recovery Glacier in the Weddell Sea Embayment). Geological constraints on the distribution of ice rises and rumples are discussed in Section 2.5.

2.4. Morphology and flow features

The new inventory allows evaluation of the geometric characteristics of ice rises and rumples. There is some uncertainty in these attributes because the size of the features is often close to or even smaller than the data resolutions. For their lateral extent, isle-type ice rises are typically wider than several kilometers (Table 1), with areas ranging between 10 and 10^3 km^2 (Fig. 4a). Promontory-type ice rises have similar dimensions, but defining their upstream extent is often difficult. In contrast, ice rumples rarely extend more than a few kilometers and generally have areas less than ~10 km^2. In terms of their vertical extent, most ice rumples are only a few meters higher than the ice-shelf surface, whereas ice rises are typically 10–310 m higher than the adjacent ice shelves and streams (Fig. 4b, Table 1). Nevertheless, ice rises and rumples are of comparable thickness (Fig. 4c), meaning that the bed elevation of most ice rumples is lower than that of a typical ice rise. Except for a few cases, isle-type ice rises have beds below sea level, and most that have been mapped have relatively smooth beds (Fig. 2). The overall shape of ice rises and rumples depends on environmental and physical conditions such as basal shear stress (related to the bed material, i.e., sediments or bedrock), ice flow speed (Fig. 4d), ice thickness (Fig. 4c), wind field, and tidal amplitude, but none of these conditions are clearly distinct between ice rises and rumples.

Crests of ice rises are often oriented nearly parallel to the regional ice flow (Fig. 1b) and perpendicular to the prevailing near-surface wind direction (Fig. 2; Lenaerts et al., 2014). Such an orientation suggests a strong geological control associated with erosion of the bed prior to the formation of the ice rises (Wilson and Luyendyk, 2006; Section 2.5). Slope changes associated with the crests are often visible as lineations in satellite imagery (e.g., Henry Ice Rise in Fig. 1a). Ice rises that have been stable for an extended period (Section 4.1) have concave shoulders on both sides of the crest, seen as near-parallel lineations in satellite imagery (Fig. 5; Goodwin and Vaughan, 1995).

In order to compensate for higher orographic precipitation (Section 2.7) and maintain in equilibrium, flanks on the windward side are generally steeper than those on the lee side (Vaughan et al., 2004). Flank slopes on most ice rises exceed ~10^{-1}° (Table 1), which is one to two orders of magnitude steeper than those on the continental ice sheet. Slopes can be even steeper on ice rises located over rough bed topography, and such slope variations in flank are often visible as lineations or variable brightness in satellite imagery (Fig. 5). Except for the largest ice rises (>~50 km long), the surface topography of ice rises is not well represented by most continent-wide digital-elevation models (DEMs). The surface topography of most ice rises is poorly mapped because of limitations in the spatial sampling of existing satellite altimetry data, particularly along the relatively steep slopes and low latitudes of coastal Antarctica. Nevertheless, accuracy of DEMs is being improved as both radar and laser altimetry techniques are used together (Bamber et al., 2009) and interferometric radar altimetry techniques are refined (Helm et al., 2014).

Similarly to the Antarctic Ice Sheet itself, flow features within an ice rise vary greatly from the flow divide to the terminus. Except for regions near the grounding zone, basal melting beneath ice rises is rare because the combination of large SMB (> ~10^{-1} m/a) and small thickness (< 1 km) ensures that the bed stays below the pressure melting point (Matsuoka et al., 2012). The ice-flow speed increases gradually towards the grounding zone, but it is less than ~20 m/a in most cases (Fig. 4d, Table 1). Fast-flowing features embedded in ice rises are rare. Exceptions include McCarthy Inlet within Berkner Island in the Weddell Sea Embayment (Fig. 6b), a fast-moving stream within Conway Ice Ridge in the Ross Sea Embayment, and Williamson Glacier within Law Dome in Wilkes Land. These all are located in bed troughs (Fretwell et al., 2013), but it is not clear whether the troughs control fast-flow locations and speeds.

Table 1
Types and characteristics of ice rises and rumples. For rows of area and below, the first number in each cell shows the median value, and two numbers in parentheses indicate the first and third quarter values.

	Ice rises (isles)	Ice rises (promontory)*1	Ice rumples	Elevated features with outcrops
Identifier in the inventory	1	2	3	4
Number	103	67	510	24
Total area (km^2)	1.18×10^5	2.07×10^5	8.52×10^3	1.88×10^3
Area (km^2)	151 (30, 560)	951 (398, 3202)	3.2 (1.2, 8.5)	16.0 (5.3, 91.2)
Longest axis length (km)*2	13.9 (6.7, 26.0)	35.9 (24.7, 63.7)	1.2 (0.4, 3.2)	3.4 (1.4, 12.2)
Orthogonal axis length (km)*2	3.0 (0, 6.1)	5.1 (0, 12.3)	0 (0, 0)	0.98 (0, 1.6)
Aspect ratio	0.17 (0, 0.28)	0.18 (0, 0.33)	0 (0, 0)	0.26 (0, 0.34)
Maximum height (m)*3	168 (56, 361)	553 (400, 659)	51 (36, 70)	55 (25, 128)
Maximum relative height from the adjacent ice (m)*3	120 (13, 306)	501 (334, 608)	2 (1, 6)	16 (8, 80)
Mean slope (degrees)*3	0.69 (0.14, 1.35)	1.26 (0.97, 1.66)	0.11 (0.07, 0.16)	0.27 (0.12, 0.97)
Maximum ice thickness (m)*3	292 (219, 375)	433 (357, 643)	372 (253, 527)	58 (31, 137)
Mean bed elevation (m)*3	−186 (−267, −119)	−178 (−311, −119)	−323 (−460, −221)	−19 (−67, −5)
Range of the bed-elevation variations within a feature (m)*3	233 (99, 421)	564 (453, 714)	15 (4, 39)	140 (58, 398)
Maximum flow speed (m/a)*3	13 (6, 23)	14 (7, 22)	67 (29, 144)	7 (5, 11)

*1 Sometimes called ice ridges or ice domes, a continuous feature of the continental ice sheet. Inland boundaries of these features are poorly defined, so spatial extent and relevant parameters are inaccurate.
*2 The orthogonal axis is defined relative to the longest axis.
*3 Surface elevation, bed elevation, and ice thickness data are from Fretwell et al. (2013). Ice-flow speed data are from Rignot et al. (2011a). Grid size of these datasets is ~1 km, so large errors may be associated with the spatial extent and other properties of the grounded features. Elevations are referenced to the GL04C geoid, which is used for the Bedmap2 dataset (Fretwell et al., 2013).

Ice flow over ice rumples is much faster than within ice rises (Fig. 4d, Table 1), causing undulating surface topography and heavily crevassed regions (Gudmundsson, 2003). Ice tends to flow more slowly across rumples that are close to larger ice rises or continental grounding zones without glaciers. Flow fields on and around rumples show complicated patterns that reflect the dynamics of the ice shelves and settings of the ice rumples (Fig. 1b).

Ice flow near the crests is of special interest because such locations are thought to be particularly suitable for ice coring to obtain minimally disturbed stratigraphic sequences for paleo-environmental interpretations. Except for a zone within a few ice thicknesses of a crest, variations of horizontal velocity with depth are approximately consistent with predictions from laminar flow theory. However, within this crest zone, longitudinal stress gradients are important. Raymond (1983) was the first to complete rigorous analysis of stresses near the crest (ice-flow divide) and he showed that, for ice with non-linear rheology, the horizontal shear strain rate there is less concentrated near the bottom and the downward ice flow is less rapid in comparison to the flanks. This ice-flow regime has important consequences for inferring depth-age relationships at flow divides (Raymond, 1983), and is now generally called the "Raymond effect". As a consequence of the Raymond effect, small shifts in the divide position have a strong effect on the vertical velocity profile (Fowler, 1992). Hindmarsh (1996) examined the dynamic response of ice divides to variations in SMB. Results showed that transient divide motion is most strongly affected by asymmetric variations in SMB halfway between the margin and the divide. Divide migration can also occur from asymmetric changes in fluxes at the margins of an ice divide (Nereson et al., 1998a). These results raise concerns that natural variability in SMB or boundary conditions can cause folding and affect the fidelity of ice-core records extracted from flow divides (Jacobson and Waddington, 2004).

Ice-rise response to environmental conditions including climate, relative sea level and ocean circulation occur over a range of timescales. Thus, the morphology and flow regime observed on ice rises today may be: (1) relicts of the expanded ice sheet during the last glacial maximum (LGM), (2) transient features that are evolving in response to changes in local ice dynamics and climate, or (3) features that are in steady state with current conditions.

2.5. Geological controls on the locations and evolution

2.5.1. Continental-shelf morphology and glacial isostatic adjustment

The locations of ice rises and rumples are determined primarily by the locations of shallower areas of the continental shelves where the ice shelf can ground (Fig. 6). This pattern is determined by the continental-shelf morphology, which has four key features. First, unlike other areas in the world, the Antarctic continental shelf is down-sloping towards the center of the ice sheet (Arndt et al., 2013). This reverse slope results from the combined effects of long-term glacial erosion (dominant effect) and subsidence (minor effect) owing to the weight of the overlying ice sheet, i.e. glacial isostatic adjustment (GIA) (Anderson, 1999). Second, faults cut across the continental shelf perpendicular to the coast (transverse faults), which tend to segment the continental shelf and often provide a route for major glacial troughs (e.g., along the western margin of the Antarctic Peninsula). Third, major faults also run parallel to the coast (longitudinal faults) which sometimes manifest as major coast-parallel troughs such as in East Antarctica (Anderson, 1999). Many of these longitudinal faults formed as a consequence of rifting of the Antarctic margin during the breakup of Gondwana in the Jurassic and are consequently long-lived structures (Anderson, 1999). Finally, overlying such tectonic structures, cycles of marine and/or glacial erosion and deposition have left their imprint following the advance and retreat of the ice sheet across the continental shelf during glacial-interglacial cycles (Wilson and Luyendyk, 2006).

These four features generate a distinctive pattern in the continental-shelf morphology. The inner shelf, closer to the ice sheet, has generally been eroded by ice during periods of greater ice extent, but during

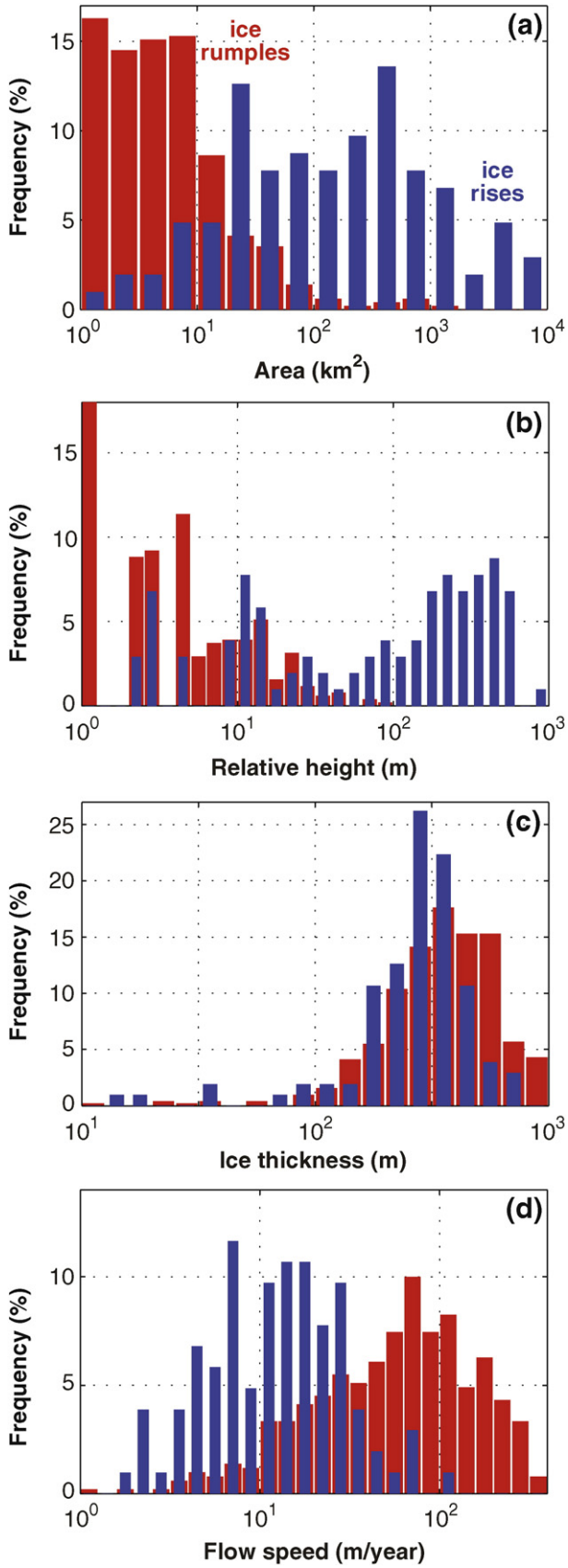

Fig. 4. Population characteristics of ice rises and rumples. Panels show histograms of (a) area, (b) relative height of the highest place (summit) of ice rises/rumples measured from the adjacent ice shelf/stream surface, (c) maximum ice thickness, and (d) maximum flow speeds within the ice rises and rumples. All abscissas have a logarithm scale, and frequency is shown in percent of a total of the 103 isle-type ice rises and 510 ice rumples inventoried in this study (Table 1, Appendix A).

times of less ice extent marine deposits can cover the crystalline bedrock. In contrast, the middle and outer shelves are dominated by depositional sequences, primarily of glaciogenic sediment that form shallow banks (e.g., Pennell Bank in the outer Ross Sea; Fig. 6a). Banks may also consist of remnant geological structures that are left upstanding after erosion on either side by paleo-ice streams. Ice rises tend to be located on these banks or on bedrock highs. For example, Roosevelt Island is grounded on an oblong seabed plateau 150–350 m below sea level, about 150-km long and 70-km wide (Fig. 6a). Berkner Island is located on part of an extensive shallow seabed plateau, which may have been completely covered by grounded ice when Berkner Island was larger in the past (Fig. 6b; Bentley et al., 2014). In contrast, its landward side has seabed troughs more than 1000-m below sea level (Fretwell et al., 2013). Longitudinal troughs can create isolated areas of high seabed on the outer parts of the continental shelf.

As well as continental-shelf morphology, another key factor controlling the formation of an ice rise or ice rumple is water depth. During glacial-interglacial cycles, global-mean sea level is predominantly governed by changes in global ice volume. However, local water depths will be modulated by GIA, which describes the deformation of the solid Earth and geoid (sea-surface height) in response to regional changes in ice loading (Farrell and Clark, 1976; Whitehouse et al., 2012). The viscous nature of the mantle means that this deformational response can take thousands of years to reach equilibrium. Therefore, following a decrease in ice mass, the subsequent gradual uplift of the seabed combined with lowering of the sea surface due to the decreased gravitational attraction of the smaller ice sheet both act to reduce water depths beneath an ice shelf, potentially leading to the formation of an ice rise.

The geology under an ice rise can reflect conditions before the current ice cover. Marine sediment might be present under many ice rises, as suggested by the typical smoothness of the bed (Fig. 2). However, direct sampling has been made only at two sites. Berkner Island (Fig. 6b) has enigmatic well-sorted quartz sand, interpreted to be aeolian in origin but of unknown age (Mulvaney et al., 2007). This sand was recognized as being similar to a widespread unit found in marine cores from the southern Weddell Sea (Rex et al., 1970). Crary Ice Rise in the Ross Sea Embayment (Fig. 6a) is underlain by microfossil-bearing marine sediments (Bindschadler et al., 1990).

2.5.2. Mechanisms of ice-rise formation and their geological imprint

The previous section outlined how geological and geophysical processes can influence the formation and location of ice rises; namely tectonics, erosion, sedimentation, and GIA. Over shorter timescales, ice-rise evolution is mainly controlled by ice dynamics, sea level, and climate. Here, we classify four main ways in which ice rises might evolve. Ice rumples can evolve similarly but presumably over shorter timescales, because most of them are only several meters higher than the surrounding ice shelf (Fig. 4b). Transitions between ice rises and rumples are poorly understood, however (Section 5.3).

1. Long-term stable

Ice rises that were already present as ice rises during periods with an expanded ice sheet are termed here, 'long-term stable' (Fig. 7a). These ice rises remain stable and were not overrun by the ice sheet at least during the last glacial cycle. An example of this type of ice rise is Berkner Island, which remained an independent center of ice flow during the last glacial cycle (Section 4.3).

2. Deglacial emergent

Under most circumstances, a retreating ice sheet implies thinning and retreat of the grounded ice and increasing flotation of the ice margin over the continental shelf. However, some ice may remain grounded on a bank of relatively high bed topography resulting in formation of a 'deglacial emergent' ice rise surrounded by an ice shelf (Fig. 7b). Ice rises can emerge similarly when the sea level rises (independent of

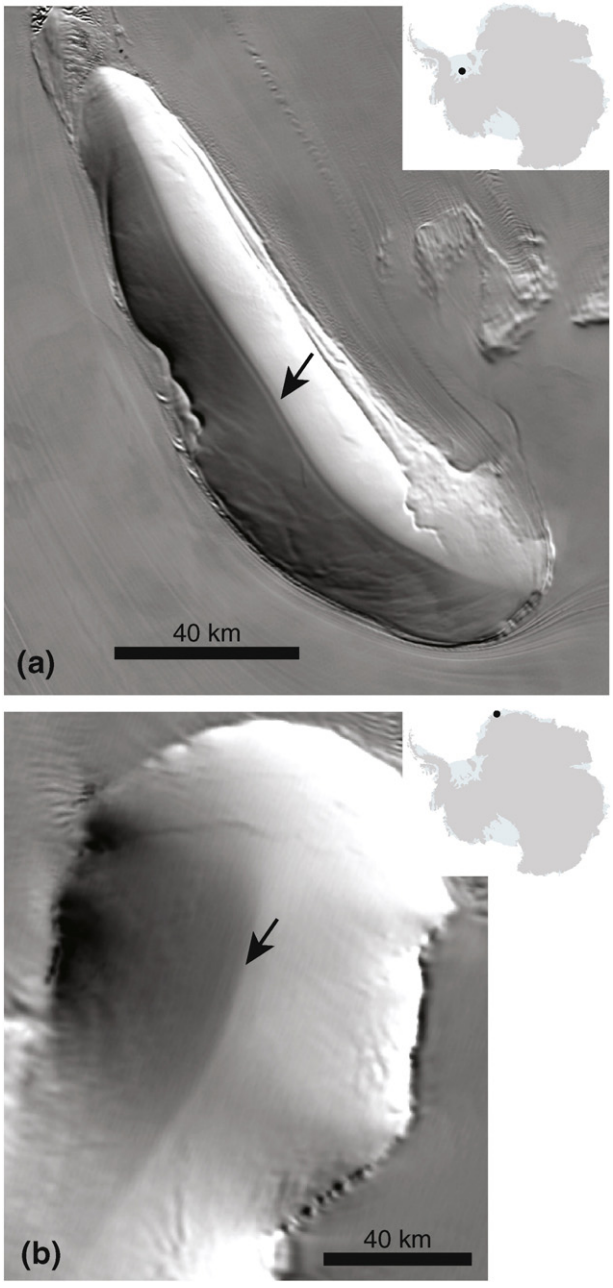

Fig. 5. Near-parallel lineations (shown with arrows) along the ice-flow divide detected by MODIS satellite imagery (Haran et al., 2005; Scambos et al., 2007). Other lineations in the flank are often associated with the slope changes. (a) Korff Ice Rise in the Weddell Sea (Smith, 1986), which has a (single-peaked) Raymond arches (J. Kingslake, unpublished data). (b) Halvfarryggen Ridge in Dronning Maud Land, which has double-peaked Raymond arches (Drews et al., 2013). For Raymond arches, see Section 4.1.

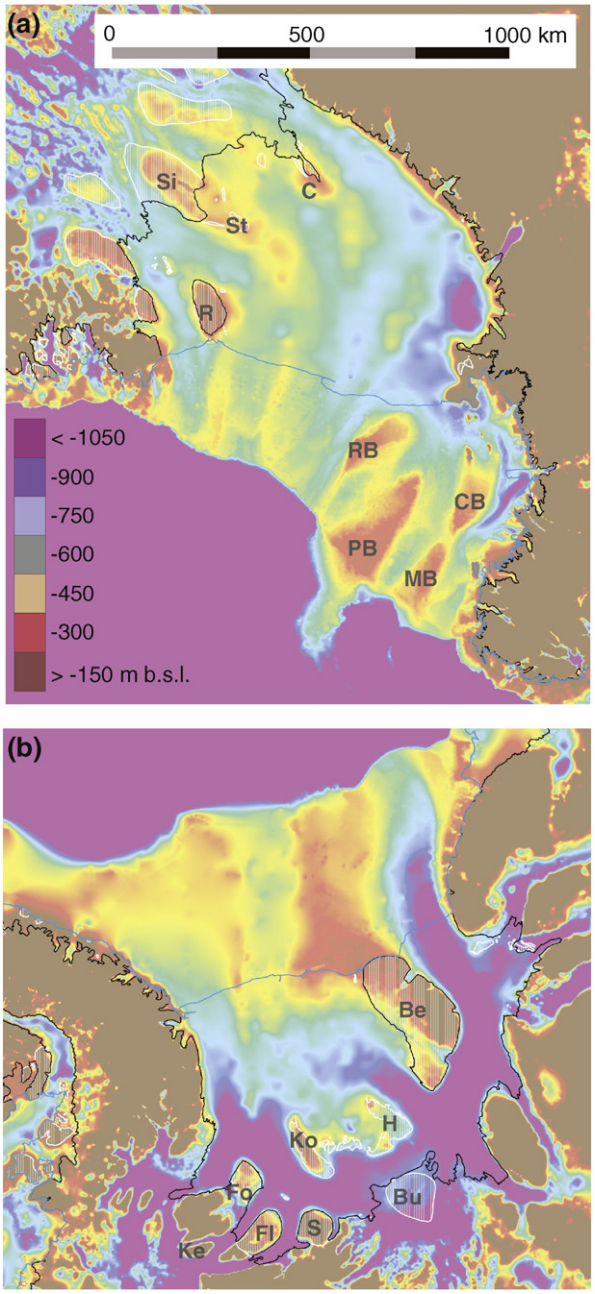

Fig. 6. Elevated bed topography beneath ice rises and rumples in the Ross (a) and Weddell (b) Sea Embayments. Bed elevations are referenced to the GL04C geoid (Fretwell et al., 2013); geoid heights are ~40 m in the Ross Sea and ~20 m in the Weddell Sea. Outlined are the grounding zone (black; Bindschadler et al., 2011) and current ice-shelf's calving front (blue; Scientific Committee on Antarctic Reseach, 2012). Inventoried ice rises and rumples (Appendix A) are hatched, and labels are given to major ice rises. In Panel (a), labeled are Siple Dome (Si), Roosevelt Island (R), Crary Ice Rise (C), and Steershead Ice Rise (St), as well as likely locations of ice rises during the LGM (Shipp et al., 1999): Crary Bank (CB), Mawson Bank (MB), Pennell Bank (PB) and Ross Bank (RB). In panel (b), labeled are the current ice rises and rumples: Berkner Island (Be), Henry Ice Rise (H), Korff Ice Rise (K), Bungenstock Ice Rise (Bu), Skytrain Ice Rise (S), Kealey Ice Rise (Ke), Fletcher Promontory (Fl), and Fowler Peninsula (Fo).

deglaciation); we include such cases in this type as well. Possible examples include Siple Dome and Roosevelt Island (if they were not long-term stable, Section 4.2).

3. GIA emergent

A thinning ice sheet may reach flotation to form an ice shelf, but subsequent post-glacial rebound may lead to re-grounding of the ice on elevated seabed to form an ice rise, here called a 'GIA emergent' ice rise (Fig. 7c). Similarly, sea-level lowering (occurring independently of GIA) can also lead to the emergence of an ice rise; we include such cases in this type as well. A possible example is Bungenstock Ice Rise in the Weddell Sea Embayment (Section 4.3).

4. Glaciological emergent

A climatic or ice-dynamic perturbation of an ice shelf or one of its feeder ice streams and glaciers may cause the ice shelf to thicken and re-ground on shallow areas of the seabed, forming a 'glaciological emergent' ice rise (Fig. 7d). Possible examples include Crary and Steershead

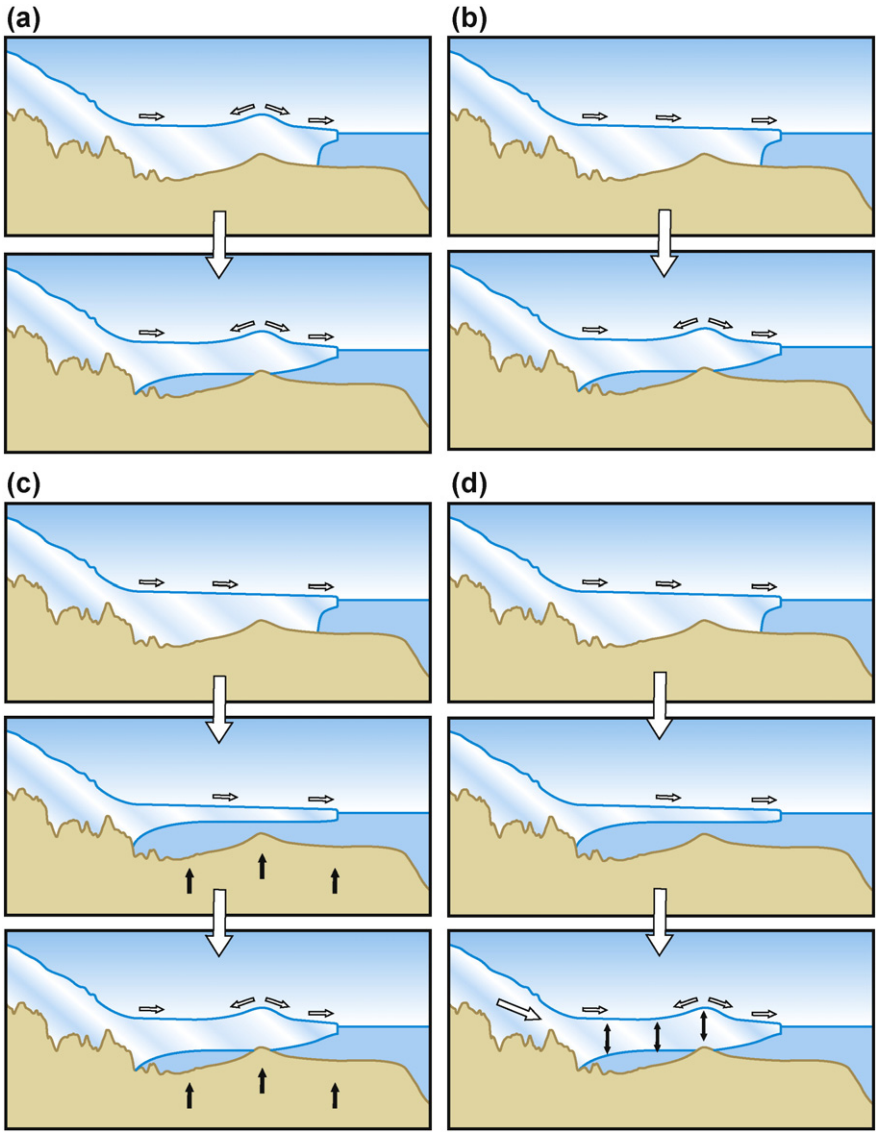

Fig. 7. Possible formation mechanisms for isle-type ice rises. (a) Long-term stable. (b) Deglacial emergent. (c) GIA emergent. (d) Glaciological emergent. For each case, the evolution is shown in scenes connected by large open downward arrows between panels. Open arrows within individual panels illustrate the direction of ice flow, whereas solid black arrows illustrate the emerging bed associated with GIA (c) and a thickening ice shelf (d). Corresponding changes of ice elevation are shown in Fig. 8.

Ice Rises in the Ross Sea Embayment that grounded in the last millennium (Section 4.2).

These four mechanisms of ice-rise formation lead to distinct age-altitude trajectories (Fig. 8). These may be recorded in terrestrial glacio-geological records of change such as those based mainly on cosmogenic isotope analysis of erratic boulders deposited on nunataks located upstream of ice rises. The first two mechanisms (cases 1 and 2, Fig. 7a and b) cause a progressive thinning of ice with time (declining age-altitude trajectory). The latter two (cases 3 and 4, Fig. 7c and d) cause a reverse age-altitude trajectory as GIA or climatic/ice-flow effects cause a re-grounding of the ice shelf and subsequent re-thickening. Records resembling the simple declining age-altitude trajectory are widespread in areas upstream of ice rises, for example at the Ford Ranges, upstream of the Sulzberger Ice Shelf (150°W) where abundant small ice rises exist today (Fig. 3, Stone et al., 2003). Other examples are found in the Ellsworth Mountains next to the Rutford Ice Stream, which flows between Fletcher Promontory and Skytrain Ice Rise in the Weddell Sea Embayment (Bentley et al., 2010). In contrast, records suggesting a reversal of the age-altitude trajectory have been found on nunataks upstream of former ice shelves, including Larsen A in the Antarctic Peninsula, which formed about 1400 years before present (1.4 ka BP) but collapsed in the past 50 years (Balco and Schaefer, 2013). Such a reverse pattern may be common, particularly if the thickening occurred recently. It is not yet possible to determine the proportion of the different pattern types because evidence has not yet been systematically sampled around the continent and we do not yet have an efficient way to sample subglacial bedrock for exposure-age dating.

Concerning the existence of former ice rises, seabed morphology mapped with swath bathymetry has shown an assemblage of ice-rise-related features such as grounding-zone features around the margins of seabed highs or banks that show evidence of radial slow flow (Shipp et al., 1999). However, the origin and timing of these features is not always clear, because shallow areas of the shelf can be modified by iceberg furrows during deglaciation. Shipp et al. (1999) identified several former potential ice-rise locations by interpreting seabed morphology and using seismic evidence of sediment pinch-out against the banks (Section 4.2). Ice rises have likely formed and disappeared throughout many glacial cycles, perhaps having played significant

roles in ice-sheet evolution since the formation of the East Antarctic Ice Sheet at the Eocene-Oligocene boundary (34 Ma BP). Ancient ice rises likely had a very different spatial distribution from that of today.

2.6. Interactions with adjacent ocean and ice shelf

Elevated seabed topography around ice rises and rumples can modify ocean circulation, which in turn can affect basal-melt/freeze patterns in the vicinity of the ice rises and rumples. In this section, we discuss ice–ocean interactions in the context of ice rises and rumples.

2.6.1. Oceanography of the Antarctic continental shelf

The oceanography of the continental shelves around Antarctica is controlled by the regional atmospheric forcing (Thoma et al., 2008; Dinniman et al., 2012; Zhou et al., 2014), the large-scale thermohaline circulation (Jacobs et al., 1992), and by tides (Makinson and Nicholls, 1999; Joughin and Padman, 2003; Padman et al., 2003).

The temperature of ocean water beneath ice shelves varies greatly around the continent. In most of the continental-shelf areas, the ocean temperature is close to the surface-water freezing point (about −1.9 °C) (e.g., Hellmer and Jacobs, 1992; Nicholls et al., 2001; Hattermann et al., 2012). Here, narrow oceanic fronts situated over the continental-shelf break separate these cold shelf waters from deep warm water in the Southern Ocean (Jacobs et al., 1992; Stewart and Thompson, 2015). In the Bellingshausen and Amundsen Seas, weaker fronts are less effective at preventing off-shelf waters from invading the continental shelves, and shelf temperature can reach as high as +1 °C (Jenkins et al., 2010b). Influx of warm deep waters is controlled by how easily the warmer, off-shelf waters can cross the shelf break to enter the continental shelf (Thoma et al., 2008; Nost et al., 2011; Hattermann et al., 2014), and also by how efficiently those waters can be cooled to the surface freezing point (Jacobs and Comiso, 1989; Nost et al., 2011; Årthun et al., 2013). Thus, the oceanographic regime of the continental shelf can be characterized as being dominated either by cross-shelf advection, or by sea-ice production on the continental shelf (Petty et al., 2013).

2.6.2. Ocean circulation beneath ice shelves

Ocean circulation beneath ice shelves is controlled mainly by the topography of the ice-shelf cavity and the regional oceanographic setting (Jacobs et al., 1992; Nicholls et al., 2009). A typical ice-shelf cavity has a two-layer water column in which flow of the upper layer is guided by contours of the ice shelf draft, whereas flow in the deep layer tends to follow contours of seabed elevation. The deep layer is the primary source of heat into the cavity. However, neither the seabed topography under most of the ice shelves nor the ice-shelf geometry are sufficiently well known to permit accurate modeling of ocean-flow paths and heat transfer at the ice-shelf base (Holland and Jenkins, 1999; Makinson et al., 2010). Instead, we consider three widely-used ocean-circulation modes beneath ice shelves: the ice-front mode (mode III in Jacobs et al., 1992), the free-convective mode (mode II), and the ice-pump mode (mode I).

The ice-front mode is induced by increased mixing due to upper ocean currents flowing perpendicular to the calving front of the ice shelf. This mode is common to all ice shelves, and typically promotes basal melting of the ice shelf within a few tens of kilometers of the calving front. It is most significant on colder regions of the continental shelf where the basal melt rates are otherwise low, in particular during the summer when the upper water column has been warmed (Zhou et al., 2014).

The free-convective mode is driven exclusively by basal melting. Melting produces a strong, buoyant, meltwater-laden (slightly lower salinity) outflow, which drives a compensating inflow at depth resulting in an open overturning circulation. This mode typically occurs beneath ice shelves with high basal melt rates, such as those in the warmer Bellingshausen and Amundsen Sea Embayments.

The ice-pump mode is forced mainly by highly saline, continental-shelf water that drains under gravity into areas beneath ice shelves. Since it is formed by sea-ice production, the water flowing into the cavity has a temperature near the surface freezing point (−1.9 °C). As it flows close to the generally landward-deepening seabed (Fig. 2), the freezing point of the saline water increases with the increasing depth by ~0.75 °C/km. The seabed near the grounding zone of the continental ice sheet can be up to 1.5 km below sea level (Fretwell et al., 2013), resulting in a freezing point of ~ −3 °C. Inflowing water at the surface freezing point can therefore melt ice at the ice-shelf base, and the resulting meltwater-rich water, with a temperature below the surface freezing point, is called ice-shelf water. The ice-shelf water is buoyant and flows up the ice-shelf base. As the hydrostatic pressure reduces with upward motion, the ice-shelf water can become super-cooled with respect to the local freezing point and form ice crystals in the water column. When the flow slows, typically where the slope of the ice-shelf base decreases, the ice crystals can precipitate out and form marine ice, which accretes to the base of the ice shelf. The ice-pump mode is typical of cold-regime continental ice shelves with low basal melt rates.

2.6.3. Basal accretion and melting of ice shelves

All three circulation modes described above can contribute to ice-shelf basal melting, and enhanced basal melting is localized near ice-sheet grounding zones (Depoorter et al., 2013; Rignot et al., 2013). However, only the ice-pump mode contributes significantly to accretion beneath ice shelves. This mode effectively pumps ice from deeper regions and fills rifts and basal crevasses with marine ice (Fricker et al., 2001; Khazendar et al., 2001). The accumulated marine-ice layer can make up one third of the ice-shelf thickness (Craven et al., 2009). Such thick marine-ice layers affect ice-column rheology (Lange and MacAyeal, 1986) and ice-shelf integrity by infilling basal crevasses (Glasser et al., 2009).

The free-convective mode dominates ice–ocean interactions in the relatively warm Amundsen and Bellingshausen Sea coasts, while the ice-pump mode dominates in the colder Ross and Weddell Sea Embayments. However, for the numerous smaller ice shelves located over relatively narrow continental shelves, such as the Dronning Maud Land (DML) coast facing the Eastern Weddell Sea, a more complicated picture emerges that is not yet well known. A belt of such ice shelves bounded

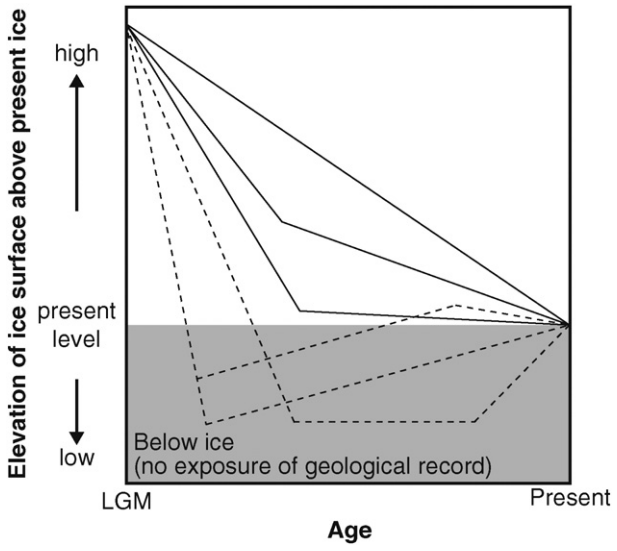

Fig. 8. Surface-elevation changes of the ice sheet upstream of ice rises, associated with the ice-rise formation mechanisms shown in Fig. 7. Solid lines show cases of long-term stable and deglacial emergent (Fig. 7a and b). Dashed lines show GIA and glaciological emergent (Fig. 7c and d). Elevation changes in the shaded area occur below the current ice surface so geological records are not exposed.

by ice rises extends along a large stretch of coast. Their calving fronts reach to the continental slope in some cases. Here, the warm deepwater circulating along the shelf break is often only a couple of kilometers away from the calving front, and ice–ocean interactions appear to be controlled by a complex superposition of all three circulation modes (Hattermann et al., 2012; Pattyn et al., 2012a). Deep ocean heat fluxes and associated melt rates near the grounding zones in these environments are controlled by Antarctic slope-front dynamics and are highly variable (Chavanne et al., 2010; Årthun et al., 2012; Hattermann et al., 2014).

The ocean circulation around Antarctica varies over time and space, and changes in large scale climatic forcing may cause regime shifts between different circulation modes. For example, a recent modeling study showed that reduced sea-ice production in a warming world can lead both to a reduction in salinity over the continental shelf and enhanced coupling between wind and ocean currents near the shelf break. Such changes would increase the warm-water inflow and basal melt of the Ronne–Filchner Ice Shelf, which is currently experiencing relatively little melting in the ice-pump mode (Hellmer et al., 2012).

2.6.4. Impacts of ice rises and rumples on ice shelves and ocean

Elevated seabed topography and modified ice-shelf shape around ice rises and rumples add more complexity to local ice–ocean interactions. Recent un-grounding of an ice rumple near the grounding zone of the Pine Island Glacier initiated deepening and widening of the ice-shelf cavity around the former rumple, which resulted in a 50% increase in basal melting near the grounding zone (Jenkins et al., 2010a). Ocean-model simulations suggest that this is due to increased separation between warm inflow and cooled outflow as the ice-bed separation has increased (De Rydt et al., 2014). However, processes are complex and the impact of ice rises and rumples on ocean circulation are not well known.

Ice rises and rumples impede nearby ice-shelf flow and affect the stress within ice shelves. The compressive stresses at the upstream margin of an ice rise exert strong buttressing forces on the discharge of inland ice (Thomas, 1979; Jezek, 1984; Doake et al., 1998; Horgan and Anandakrishnan, 2006; Braun et al., 2009; Borstad et al., 2013). In contrast, the tensile stresses at the downstream margin of an ice rise often initiate crevassing and rifting around ice rises and rumples (Figs. 1 and 2), which can propagate and destabilize an ice shelf (e.g., Hulbe et al., 2010; Humbert and Steinhage, 2011).

Ice-shelf flow often produces bands of crevasses and rifts visible in satellite imagery (Limbert, 1964; Swithinbank, 1977; Smith, 1986; Glasser and Gudmundsson, 2012). Theoretical studies suggest that ice-shelf cavities incised upwards into an ice shelf can channelize ice–ocean interactions (Gladish et al., 2012; Sergienko, 2013). Indeed, ice rises and rumples in the Larsen C Ice Shelf produce bands of marine ice downstream (Holland et al., 2009), which affect stability of the ice shelf (Jansen et al., 2013; Kulessa et al., 2014). The overall impact of such structural changes, marine-ice accretion and channelized ocean flow remain poorly understood in the context of ice-shelf dynamics and the role of ice rises and rumples.

2.7. Local climate and surface mass balance

The main source of mass input to an ice rise is local snow accumulation. This implies that local surface mass balance (SMB) strongly controls ice-rise evolution. The topographic signature of an ice rise on a relatively flat ice shelf impacts the local and regional SMB pattern over ice shelves (Lenaerts et al., 2014). However, owing to their small size, individual ice rises are not well represented in most atmospheric-circulation models, which hampers modeling of the magnitude and spatial patterns of SMB across ice rises and over adjacent ice shelves.

Two distinct wind systems are in operation in coastal Antarctica. One is the downslope katabatic winds from the Antarctic Plateau towards the coast. These follow large-scale topography and are thus usually directed from south to north, but slightly deflected to the west by the Coriolis effect (Van Lipzig et al., 2004). It results in surface winds prevalently from the southeast in Antarctica. The other wind is related to synoptic-scale storms, which transports moist air inland (e.g., Gorodetskaya et al., 2013; Lenaerts et al., 2014). As the moist air rises on the windward side of ice rises, it condenses resulting in precipitation. The pattern of SMB around an ice rise is dominated by orographic precipitation on the upwind side during synoptic storms (Fig. 2).

In-situ observations and regional climate models indicate that SMB on the windward side of ice rises can be 2–5 times higher than that on the adjacent ice shelf (Fernandoy et al., 2010; Lenaerts et al., 2012; Drews et al., 2013). On the downwind side of the ice rise, however, downslope flow warms and dries the air adiabatically; here SMB is less than on the ice shelf (Lenaerts et al., 2014). Also, anomalously low SMB can occur near the crest, as a result of wind erosion (Lenaerts et al., 2014; Drews et al., 2015). SMB patterns are also affected by small variations in the wind field and associated drifting snow (King et al., 2004; Lenaerts and van den Broeke, 2012). Other topographic effects include (1) horizontal divergence of the wind field on the upwind side, (2) strong downslope acceleration on the downwind side, (3) increased snow erosion associated with the high wind speeds, and (4) increased snow sublimation by relatively dry air on the downwind side of an ice rise. For example, spatial patterns of SMB observed over Lydden Ice Rise in the Brunt Ice Shelf (20°W) are reproduced well with a simple airflow model coupled to a blowing snow transport parameterization, under the assumption that precipitation variations across the ice rise are negligible (King et al., 2004).

Observations of SMB over ice rises are complicated by significant spatial variations in the near-surface density and vertical strain. First, consider density. Snow density is often assumed to be spatially uniform and SMB is assumed to be proportional to observed stake heights. However, analysis of shallow (3-m long) firn cores across three ice rises in the Fimbul Ice Shelf indicate that variations in surface snow density over an ice rise can exceed 35% (J. Brown and K. Matsuoka, unpublished data). This variation results in a discrepancy of calculated SMB from stake measurements by up to ~20% when compared with calculations based on the mean of all density measurements. Assuming uniform density is also problematic when estimating SMB using near-surface radar reflectors (assumed to be isochrones), because the density affects radio-wave propagation speed and hence the calculation of depth to the reflector. Spatial variations in vertical strain are also a concern because they violate the so-called “shallow-layer approximation” (i.e. the local layer thickness is proportional to the SMB for the corresponding periods (Waddington et al., 2007)). This assumption is often used to derive SMB but it can be particularly problematic over ice rises owing to the combination of relatively small ice thickness and large SMB (Vaughan et al., 1999; Drews et al., 2015), and basal melting near the grounding zone (Catania et al., 2010; Matsuoka et al., 2012).

3. Impacts of ice rises and rumples on ice-sheet dynamics

Ice rises and rumples interact with the seabed (Section 2.5), atmosphere (Section 2.7), ocean, and ice shelves (Section 2.6.4), and feedbacks with these components can alter the dynamics and morphology of ice rises and rumples (Section 2.4). Ultimately, these feedbacks especially those within ice shelves cause buttressing, which regulates the grounding-zone position and reduces fluxes from the ice sheet (Gagliardini et al., 2010). However, only a few studies have evaluated the interplay between ice rises, grounding zones, and evolution of the ice sheet. Prognostic modeling studies have so far been limited to synthetic cases.

Thomas (1973a, 1973b) used measurements of strain rates to calculate the buttressing exerted by the MacDonald Ice Rumples in the Brunt Ice Shelf and concluded that the buttressing effect is inversely proportional to the distance from the ice rumples. Buttressing from Crary Ice Rise reduce the horizontal spreading rates in front of the Mercer and

Whillans Ice Streams by several orders of magnitude compared with that which would occur without the ice rise (Thomas and MacAyeal, 1982). The resistance exerted by Crary Ice Rise accounts for about 50% of the buttressing on the Whillans Ice Stream (MacAyeal et al., 1987). Using a finite element model, Schmeltz et al. (2001) showed that ice rises reduce the discharge from Pine Island Glacier. Similar impacts were found for Bawden and Gipps Ice Rises in the Larsen C Ice Shelf; these two small ice rises near the calving front slow the flow of the ice shelf (Borstad et al., 2013). Current ice-flow models cannot replicate observed pattern of flow of ice shelves around ice rises and rumples that are not charted in the Bedmap2 data but visible in satellite imagery (Fürst et al., 2015).

The net effect of an ice rise on the flow of grounded ice depends on the ice rise's location within an ice shelf. For example, ice rises in a well-protected inlet of the Ronne–Filchner Ice Shelf have very small influences (Schmeltz et al., 2001). Similarly, the disappearance of an ice rumple from Thwaites Glacier's floating ice tongue increased flow speeds at the grounding zone on either side of the ice tongue, but the maximum speed of the tongue remained unchanged (Rignot, 2008). Furthermore, a model study showed that potential un-grounding of a local grounding feature near the front of the slowly-moving eastern part of the Thwaites glacier tongue seems to have a little influence on mass-balance projection of the glacier (Joughin et al., 2014).

Favier and Pattyn (2015) were the first to model the progression from a promontory-type ice rise to an isle-type ice rise as the grounding zone retreats beyond a locally-elevated seabed (a seamount). The presence of an ice rise affects the timing of deglaciation by exerting buttressing on the ice sheet, but in steady state grounding-zone positions only slightly differ when the seamount and associated ice rise are present or absent. They point out that promontory-type ice rises are transient features during the deglaciation, whereas isle-type ice rises are more stable. In steady state, the ice shelf seaward of the ice rise is much thinner than on the landward side, consistent with an observation (Fig. 2). This may explain why many isle-type ice rises limit the seaward extent of the ice shelf (Fig. 3). Model experiments by others over glacial-interglacial cycles have also demonstrated that ice rises play an important role both in the growth and collapse of the ice sheets (Pollard and DeConto, 2009, 2012). Although it is clear that ice rises influence the flow of the grounded ice, the controls are complicated, and depend on the shape and distribution of ice rises and seamounts.

Isle-type ice rises and ice rumples play a role in modulating the development of a marine-ice-sheet instability (MISI). A MISI occurs when the initial thinning and retreat of the grounding zone causes thinning and floating of the upstream part of the ice sheet on an inland-deepening bed (Weertman, 1974; Schoof, 2007). Goldberg et al. (2009) first examined the influence of a local grounding on a seamount, and found that its presence can stabilize MISI-induced grounding-zone retreat, and in fact, perhaps reverse the process, resulting in unstable advance. Bradley et al. (2015) invoke this process to explain GPS-observed solid Earth deformation in the Weddell Sea Embayment (Fig. 6b), concluding that the grounding zone must have retreated upstream of Bungenstock Ice Rise during the late Holocene and then subsequently re-advanced to its current unstable position following GIA-induced re-grounding of the ice shelf landward of the ice rise. Favier et al. (2012) examined the effects of ice-rumple emergence by forcing a model with an abrupt decrease in sea level. In this case, the ice shelf grounded on a seamount, producing first an ice rumple. The buttressing decreased the ice-shelf speed and the ice-sheet's grounding zone advanced until it merged with the rumple. Once the ice rumple had been subsumed by grounded ice, the grounding zone did not revert back to its original position even if the sea level was increased back to the initial value. Despite these advances, models have not yet produced a steady configuration where ice rises or rumples exist within ice shelves, except for a recent work on a stable isle-type ice rise during deglaciation (Favier and Pattyn, 2015).

Additional model experiments by Schmeltz et al. (2001) showed that an ephemeral ice rumple during low tides has only a small influence on the flow of the ice shelf. The results suggest that thickening beyond a critical value (perhaps sufficient to maintain grounding over tidal cycles) is necessary to have a significant buttressing. However, conditions for sustained grounding are a threshold problem, which is poorly understood. None of the above-mentioned model experiments were designed to examine impacts of ice rises and rumples separately. Also, the model used here is diagnostic, not transient, which is not fully capable to capture the effects of grounding zones. Additional work is needed to understand the details of the impact of ice rises and rumples on grounding-zone dynamics.

4. Records and dynamic roles of ice rises during Holocene

Ice rises and rumples have impacted on the Holocene deglaciation of Antarctica. The glaciological imprints of such changes from ice rumples are advected downstream, but those from ice rises remain locally in their thermal structure (Bindschadler et al., 1990) and englacial stratigraphy (Conway et al., 1999). Owing to the relatively thin ice (ice thickness H = m; Table 1) and large SMB around the Antarctic coast (b > ~0.1 − 0.3 m/a; Van de Berg et al. (2006) and Lenaerts et al. (2014)), the characteristic ice-flow timescale T (= H/b; Cuffey and Paterson (2010)) of ice rises is typically several thousand years or shorter. Thus, ice rises can potentially retain an imprint of past evolution for several millennia. Furthermore, as most ice rises are frozen to their beds (except near the grounding zone), ice near the bed can be much older than the several millennia, potentially well beyond the LGM (Mulvaney et al., 2007; Bertler et al., 2014; Mulvaney et al., 2014). Glaciological imprints over shorter periods (less than a millennium) can also be seen in the shape of satellite-observed flow stripes on the ice shelf. These features generated near ice rises and rumples are then advected downstream by flow of the ice shelf (Fahnestock et al., 2000) and have been used to infer temporal changes in the relative contributions of adjacent ice-flow units downstream of ice rises (Hulbe and Fahnestock, 2007).

In this section, we first describe the physical mechanisms that generate englacial stratigraphy, and how they can be used to constrain evolution of ice rises and their vicinities (Section 4.1). We then review current knowledge of Holocene deglaciation in four sectors of Antarctica, emphasizing the records and dynamic roles of ice rises (Sections 4.2–4.5). The lesser-explored regions that constitute half of the Antarctic coast are briefly discussed in Section 4.6.

4.1. Constraints from englacial stratigraphy

Dated ice cores from ice rises can be used as dipsticks to extract histories of ice thickness. The thickness of an annual layer (in ice equivalent, the derivative of the depth-age relationship) depends not only on its initial thickness (the annual SMB, when it was deposited) but also on the cumulative vertical strain since it was deposited. Therefore, when the history of SMB can be determined independently, the history of ice thickness can be inferred (Waddington et al., 2005).

Radar-detected englacial stratigraphy (Fig. 2) also provides a powerful constraint on the evolution of ice rises. The shapes of the observed reflectors (assumed to be isochrones) are replicated using numerical ice-flow models for several hypothetical cases, and comparison to observed features is used to judge the likelihood of each case. Histories of ice flow can be extended further back in time when the radar reflectors can be dated by tracking them back to an ice-core site.

For ice rises, modeling efforts focus on the near-crest or near-summit region (ice-flow divide). The nearly flat surface in the divide vicinity makes the driving (gravitational) stress applied to that ice much smaller than that applied to flank ice, and the main stress is the longitudinal stress caused by the flank ice tugging on the divide ice. Owing to

Glen's power flow law, ice near the bed within two to three local ice thicknesses from the divide is much stiffer than the ice at a corresponding elevation in the flank, which impedes downward flow. This divide-specific flow characteristic was predicted by Raymond (1983) and is frequently called the "Raymond effect". When certain conditions (outlined below) are satisfied, the Raymond effect often causes divide ice of a given age to be at shallower depths than the flank ice, causing "Raymond (upward) arches" in the isochronous ice stratigraphy (Figs. 2 and 9a). Raymond et al. (1995) first observed local upward radar reflectors beneath the divide of Siple Dome, which can be associated with a local low in SMB and/or local flow regime at a divide (i.e. Raymond effect). Nereson et al. (1998b) used it to analyze migration of the divide, assuming that it is a proxy of the divide position in the past regardless of its cause. Vaughan et al. (1999) demonstrated that these causes can be distinguished using a simplified ice-flow model; a persistent local low in SMB causes arch amplitudes that increase with depth linearly, while amplitudes of Raymond arches increase quadratically with depth. Using this method, upward arches found at 20–80 m depths in Fletcher Promontory were diagnosed as Raymond arches (Vaughan et al., 1999). Conway et al. (1999) first analyzed the depth profile of the Raymond-arch amplitudes to determine the onset of timing and thinning at Roosevelt Island.

Raymond arches become distinctly visible in radargrams after one characteristic time period T, and reach a steady state after a few T (Martin et al., 2009b). The amplitude of the Raymond arches increases from the top to about two thirds of the ice thickness, and decreases from there to the bottom of the divide (Fig. 9b). The shape of (the stack of) Raymond arches has been used to infer the onset timing of divide flow and ice thickness changes (Conway et al., 1999; Martin et al., 2006), divide migration (Nereson and Waddington, 2002), and stochastic variations in divide position (Hindmarsh, 1996; Martin et al., 2009b). However, the shape can also be modified by (1) the spatial SMB patterns (Nereson et al., 2000; Nereson and Waddington, 2002; Drews et al., 2013, 2015), (2) the temperature profile through the ice column and geothermal flux (Hvidberg, 1996; Nereson and Waddington, 2002), (3) variations in ice rheology (Martin et al., 2006; Pettit et al., 2007, 2011) and (4) basal sliding (Pettit et al., 2003; Martin et al., 2009b). In fact, Raymond arches will not form under conditions of strong basal sliding (Pettit et al., 2003), but vertically-oriented alignments of ice crystals should increase the arch amplitude (Pettit et al., 2007; Martin and Gudmundsson, 2012).

R.C.A. Hindmarsh and G.H. Gudmundsson observed radar-detected complex arches in the bottom one third of the ice beneath the divides of Fletcher Promontory and Kealey Ice Rise during the 2005–6 Antarctic field season. The stratigraphy includes a combination of two anticlines; one is like Raymond arches, and the other is a downward curving fold (syncline) in the central part (Fig. 9a). Also, the tail of the larger Raymond arches often shows small flanking synclines (Fig. 1 in Hindmarsh et al., 2011). Parrenin and Hindmarsh (2007) demonstrated that flanking synclines can arise as a consequence of sharp horizontal changes in the ice viscosity. Martin et al. (2009a) argued that these synclines in the central and flank parts of the Raymond arches can form as a result of the development of crystal alignments under stress configurations unique to the divide (i.e. Raymond effect), so hereafter we call this stratigraphy "double-peaked Raymond arches". Martin et al. (2009a) also showed that the development of crystal alignments could also explain the concave shoulders observed in the surface topography near some divides, which are visible as two near-parallel lineations in satellite imagery (Fig. 5; Goodwin and Vaughan, 1995). It takes at least 1 T to develop concave shoulders and 2 T to develop the double-peaked Raymond arches (Martin et al., 2009a). The different time scales might explain why near-parallel satellite lineations are visible on Korff Ice Rise (Fig. 5a) but radar-detected stratigraphy shows single-peaked Raymond arches (J. Kingslake, unpublished data).

Many Raymond arches in ice rises have not fully responded to Holocene deglaciation, because a steady state is reached progressively later

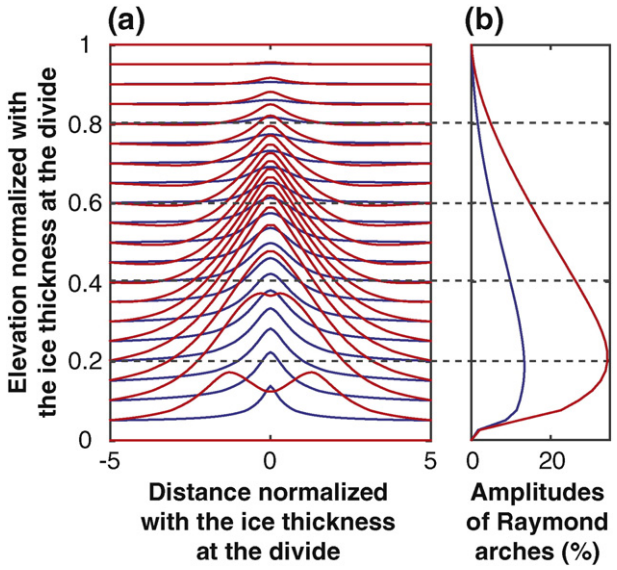

Fig. 9. Properties of Raymond arches. (a) Cross section of modeled isochrones. (b) Depth variations of the arch amplitudes relative to the ice thickness at the divide. In both panels, blue shows a case of isotropic ice resulting in single-peak Raymond arches, and red shows a case of anisotropic ice induced by development of ice-crystal alignments resulting in double-peaked arches. The figure shows steady-state model results presented in Fig. 11b of Martin et al. (2009a).

at greater depths, and thus the entire stack of the Raymond arches reaches steady state only after ~10 T in anisotropic ice (Martin et al., 2009a). Where the Raymond arches have not yet reached steady state, their shape is affected by the evolution of the ice mass (Nereson et al., 1998a, 1998b; Nereson and Raymond, 2001). The interpretation of histories of ice dynamics from the shape of the Raymond arches is not always unequivocal. Ambiguities come from uncertainties in the flow law (i.e., Glen's Index, Drews et al., 2015), the evolution of alignments of ice crystals (Martin and Gudmundsson, 2012), and SMB history (Waddington et al., 2005).

Vertical velocities in ice rises have been measured directly using phase-sensitive radar (Gillet-Chaulet et al., 2011; Kingslake et al., 2014) or borehole strain measurements (Pettit et al., 2011), which allows one to constrain Glen's Index and assess the evolution of the ice rises more reliably from the shape of the Raymond arches. Nevertheless, Glen's Index changes with time, as the crystal alignments change. The Law Dome ice core shows that ice-crystal alignments can be variable even in the dome of the ice rise (Wang et al., 2002).

Raymond arches have been found at all ice rises investigated so far, except for Conway Ice Ridge in the Ross Sea Embayment (see Section 4.2). Therefore, Raymond arches are relatively common on ice rises, but they have not been observed beneath the continental divides of the Antarctic Ice Sheet (Neumann et al., 2008; Fujita et al., 2012). This absence may be explained by a combination of long characteristic time (10–20 ka for West Antarctica and more than 100 ka for East Antarctica), basal melting owing to small SMB and thick ice (Pattyn, 2010), and possible divide migration during the Holocene beyond the lateral range of the Raymond effect, which is only a small fraction (1–2%) of the flowline from the divide to the coast. In contrast, on ice rises, a combination of thin ice and large SMB keep the bed frozen, creating a significant Raymond effect over a relatively long range (10–15% of their flow line). Also, characteristic times are at least one order of magnitude shorter than the continental divides. These conditions make the Raymond arches in ice rises more persistent and useable in constraining regional evolution.

4.2. Ross Sea

Onshore and offshore studies show that an expanded, grounded ice sheet occupied the Ross Sea during the LGM, which raises the question: did the Ross Embayment have ice rises during the LGM? On the western continental shelf, north of Ross Island, troughs between four prominent banks (Ross, Pennell, Crary, and Mawson; Fig. 6a) show evidence of mega-scale glacial lineations, grooves, and grounding zone wedges, but relatively few glacial geological features occur on the banks themselves. One explanation is that these banks supported ice rises that were frozen to the bed (Shipp et al., 1999). It is thought that there were ice rises during an early retreat of the ice sheet but that the ice rises disintegrated when the Ross Ice Shelf retreated farther south in the early Holocene (Anderson et al., 2014). Early glaciological reconstructions (Hughes, 1973; Thomas, 1973b; Whillans, 1973; Thomas, 1979) recognized the possibility of such pinning points and their effect on stabilizing (or destabilizing) the expanded ice sheet.

Numerous ice rises (including inter-ice-stream ridges) and ice rumples also exist in the Ross Ice Shelf today (Fig. 3). Roosevelt Island, which is near the present ice-shelf calving front, provides a strong constraint on the deglaciation history of the region. Depth profiles of radar-detected Raymond arches indicate that divide flow started 3 ka BP, with the implication that the grounding line retreated past Roosevelt Island at this time (Conway et al., 1999; Martin et al., 2006). Preliminary results from a full-depth ice core drilled on the divide by the RICE consortium indicate a continuous record extending back 30–40 ka BP (Bertler et al., 2014).

Siple Dome, an inter-stream ridge between Kamb and Bindschadler Ice Streams, has been the site of extensive glaciological investigations, including a 1004-m-long ice core to the bed (Taylor et al., 2004). Depth profiles of age (Brook et al., 2005) and borehole temperature (MacGregor et al., 2007) have been used to infer thinning of ~350 m about 14–15 ka BP (Price et al., 2007). The shape of radar-detected stratigraphy across the dome shows that divide flow started 3 ka BP, and the divide started migrating northward 2.5 ka BP, likely because of relative changes in the activity of the bounding ice streams (Nereson and Raymond, 2001). Raymond arches in nearby Engelhardt and Shabtaie Ice Ridges have also been migrating northward over the past few thousand years; the implication is that the surface elevation of ice streams to the south have been decreasing during this period (Nereson and Raymond, 2001). In contrast, radar surveys across Conway Ice Ridge between Mercer and Whillans Ice Streams do not show evidence of Raymond arches. Rather, the englacial stratigraphy is highly disturbed and folded, suggesting that the ice ridge has been over-run by fast-moving ice in the recent past (Conway et al., 2005).

Unlike Siple Dome, Crary and Steershead Ice Rises are not relicts of the expanded LGM ice sheet, but instead they have emerged within the last millennium owing to increased discharge from Kamb and Whillans Ice Streams (MacAyeal et al., 1987; Bindschadler, 1993). Evidence from cooling trends measured in two boreholes on Crary Ice Rise have been used to estimate that grounding occurred ~1.1 ka BP at one site and 580 years ago at the other site (Bindschadler et al., 1989, 1990). Flow stripes preserved in the Ross Ice Shelf contain a rich history of interactions between ice stream, ice shelf, and ice rise over the past millennium (the time it takes for shelf ice to transit to the ocean). Numerical modeling shows (i) grounding of Crary Ice Rise ~1 ka BP, followed by stagnation of Whillans Ice Stream 150 years later and recommencement of streaming flow ~450 years ago; (ii) grounding of Steershead Ice Rise ~200 years ago followed by stagnation of Kamb Ice Stream ~50 years later (Hulbe and Fahnestock, 2007; Catania et al., 2012). This rich history of interactions between ice rise evolution and slow downs of nearby ice streams has the potential to elucidate controlling processes near grounding zones.

4.3 Weddell Sea

Offshore studies show that the Weddell Sea Embayment had a thin cover of grounded ice during the LGM, sloping very gently from the interior to the margin at the continental shelf break when it had its maximum extent (Hillenbrand et al., 2013). Marine-sediment records and cosmogenic isotope dating of outcrops (Bentley et al., 2010) show similar timings of ice-sheet retreat (~15 ka BP). This embayment has far fewer outcrops suitable for geological surveys than the Ross Sea Embayment, and offshore surveys in the Weddell Sea are often restricted by unfavorable sea-ice conditions. Glaciological imprints on ice rises therefore provide important information about Holocene deglaciation of the region.

Today, the Weddell Sea Embayment contains a diverse population of ice rises (Figs. 1, 3 and 6b). Berkner Island, Korff and Henry Ice Rises are surrounded entirely by the Ronne–Filchner Ice Shelf. Fowler Peninsula, Fletcher Promontory, and Skytrain and Bungenstock Ice Rises are inter-ice-stream ridges constituting part of the continental grounding zone, whereas Kealey Ice Rise is an inter-ice-stream ridge adjacent to tributaries of ice streams, located landward of the grounding zone. Radar surveys have been carried out on Berkner Island, Fletcher Promontory (Vaughan et al., 1999; Martin et al., 2009a; Kingslake et al., 2014), Kealey Ice Rise (Martin et al., 2014), Bungenstock Ice Rise (Siegert et al., 2013), Fowler Peninsula, and Korff, Skytrain, and Henry Ice Rises (J. Kingslake, unpublished data). Raymond arches in the radar stratigraphy have been analyzed at Berkner Island (Hindmarsh et al., 2011), Fletcher Promontory (Vaughan et al., 1999; Hindmarsh et al., 2011), and Kealey Ice Rise (Martin et al., 2014). Initial analyses show no clear evidence of Raymond arches in Henry Ice Rise, and Korff Ice Rise (Fig. 5a) is unique in that near-parallel lineations near the crest are visible in satellite images, but radar-detected stratigraphy shows single-peaked (rather than double-peaked) Raymond arches (J. Kingslake, unpublished data).

Deep ice cores have been drilled at Berkner Island (948-m long to the bed; Mulvaney et al. (2007)) and Fletcher Promontory (654-m long to the bed; Mulvaney et al. (2014)). The Berkner Island core suggests that the basal ice may be older than 120 ka and that the LGM-Holocene transition is 300–350 m above the bed (Mulvaney et al., 2007). Berkner Island has probably been persistent, constituting an independent flow divide during the LGM, though it remains unknown whether Berkner Island was an isle- or promontory-type ice rise. Initial analysis of the ice core from Fletcher Promontory also suggests that it will provide a similarly detailed record extending back at least 100 ka BP (Mulvaney et al., 2014). These two ice cores show that long histories of climate and ice dynamics can be preserved in ice rises.

Radar stratigraphy collected on Berkner Island, Fletcher Promontory and Kealey Ice Rise all suggest divide positions unchanged over an extended period. Kealey Ice Rise has double-peaked Raymond arches and corresponding near-parallel satellite lineations, which suggest that the divide position has been stable over the past 3 ka, although more recent reorganization of flow in the last century cannot be excluded (Martin et al., 2014). Berkner Island and Fletcher Promontory flow centers are triple junctions of ice crests (Hindmarsh et al., 2011). Analysis of a radar survey across the Berkner Island triple junction shows one strong Raymond arch that has been in steady state since it started forming ~4 ka BP but arches on the other ridge are muted. The survey across the Fletcher Promontory triple junction shows a clear set of arches that suggest the summit occupied this position ~5 ka BP, and has been thinning with a mean rate of 0.1 m/a. In addition, a set of well-developed, double-peaked Raymond arches exists about 3 km from the current summit of Fletcher Promontory. It is likely that the arches formed owing to development of ice-crystal alignment, but the location and shape of the arches is not completely explained by current understanding of the physics and timescales of processes (Hindmarsh et al., 2011).

In contrast, Bungenstock Ice Rise has experienced significant changes in its flow regime over the late Holocene (Siegert et al., 2013). Radar-detected stratigraphy shows surface conformable, undisrupted layering in the upper half of the ice column, but highly deformed and buckled layering in the lower half. The stratigraphic sequence suggests that the older ice was deposited upstream of the present-day ice rise and was deformed by enhanced flow, while the younger undisrupted layers were deposited after the ice rise grounded (Siegert et al., 2013). Bungenstock Ice Rise could have developed either as a promontory-type ice rise during the grounding-zone retreat, or initially as an emergent isle-type ice rise before transitioning to a promontory type as the grounding zone advanced further. Bradley et al. (2015) present GIA data and modeling results that support the grounding zone re-advance hypothesis.

4.4. Antarctic Peninsula and Amundsen Sea

The Antarctic Peninsula and Amundsen Sea regions have been undergoing deglaciation since the LGM, generally from outer-to-inner regions and north-to-south (Heroy and Anderson, 2007). Numerous ice rises in this region presumably have strong controls on the regional deglaciation pattern. In recent decades, glaciers and ice shelves around the Antarctic Peninsula and along the Bellingshausen Sea Coast (bounded by the Antarctic Peninsula and Pine Island Bay) are changing rapidly (Vaughan et al., 2003; Thomas et al., 2008), with several shelves in the Antarctic Peninsula collapsing or thinning in response to atmospheric warming (Cook and Vaughan, 2010) or thinning due to basal melting (Pritchard et al., 2012).

Satellite imagery shows two near-parallel lineations (similar to those shown in Fig. 5) near the crest of 23 ice rises in this region (Fig. 10). Modest ice thickness (population statistics $H \approx 490 \pm 200$ m; Fretwell et al. (2013)) and very high SMB ($b \approx 0.92 \pm 0.48$ m/a water equivalent; Arthern et al. (2006) and van den Broeke et al. (2006)) indicate that the characteristic time scales T are less than 500 years for 12 ice rises and 500–1000 years for six ice rises. The short characteristic times and their proximity to the coast make them sensitive indicators of recent climate- and ocean-driven dynamic change.

Detailed ground-based radar surveys have been conducted over four ice rises: Adelaide Island (or Fuchs Piedmont, Martin et al., 2009a; Kingslake et al., 2014), King George Island (Blindow et al., 2010), Latady Island, and Monteverdi Peninsula (H. Pritchard, unpublished data). Also, airborne radar surveys were flown during the British Antarctic Survey's GRADES-IMAGE project on two other ice rises. King George Island has single-peaked Raymond arches, while all the other five ice rises have well-developed, double-peaked Raymond arches (Fig. 9). The time scale for formation of double-peaked arches is 2 T or longer (Martin et al., 2009a). An implication is that conditions at these sites have been largely unchanging at least for several centuries. Furthermore, any change in the dynamics must have been very recent because more sustained change would remove the architecture of the Raymond arches.

Raymond arches detected on Adelaide Island are offset from the current topographic divide (Martin et al., 2009a). Ice-flow modeling shows that this offset is unlikely to be a steady-state asymmetry caused by sloping bed or a gradient in SMB. Instead, it is likely to have been caused by a recent and anomalous change in ice flux across one of the margins of the island, but the change is too recent to have removed the existing architecture or to have caused a new stack of arches to form beneath the current divide position. The response time of divide location to a flux perturbation at the margin is ~T/16 (Hindmarsh, 1996), which is ~25 years in this case. Additional work is needed to constrain the timing of changes more accurately and to investigate signals of changes across other divides in this region.

4.5. Dronning Maud Land

Glacial-interglacial variations of the ice-sheet margin in Dronning Maud Land (DML; 20° W - 45° E) are probably smaller than most other regions owing to its close proximity to the continental-shelf break (Mackintosh et al., 2013). Currently the DML coast consists of 1500-km of ice shelves, fed by outlet glaciers and punctuated by numerous ice rises (Fig. 3). Most ice shelves extend less than 100 km from the grounding zone to the calving front, which is close to or even beyond the continental-shelf break (Arndt et al., 2013). The area of ice shelves in this region decreased by 6.8% between 1963 and 1997, mostly in regions without ice rises and rumples near the calving front (Kim et al., 2001). This observation supports the hypothesis that ice rises generally stabilize ice shelves.

So far only seven of ~30 inventoried ice rises in DML have been investigated. These are Søråsen Ridge (10° W; A. Winter and D. Steinhage, Pers. Comm.), Halvfarryggen Ridge (7° W; Drews et al. (2013)), three ice rises near the Fimbul Ice Shelf (Blåskimen Island, Kupol Moskovskij, and Kupol Ciolkovskogo; Norwegian Antarctic Research Expeditions), an unnamed ice rise at 24° E (Matsuoka et al., 2012; Pattyn et al., 2012a), and Derwael Ice Rise (26° E; Drews et al. (2015)) both in the Roi Baudouin Ice Shelf. In addition, field and remote-sensing studies are ongoing at ice rumples in the Roi Baudouin Ice Shelf (Belgian Antarctic Research Expeditions). Many ice rises in DML have topographic ridges roughly perpendicular to the prevailing wind direction, so their influence on the regional pattern of SMB is strong (Lenaerts et al., 2014).

All seven ice rises have distinct Raymond arches, except for an unnamed ice rise at 24° E, which nevertheless has distinct arches beneath its crest but the undulated bed there prevents conclusive interpretation of its cause. Halvfarryggen Ridge has double-peaked Raymond arches (Fig. 9), and corresponding near-parallel lineations are visible in satellite imagery (Fig. 5b). Model results indicate that the divide position has been steady for at least 2.7–4.5 ka, a time period necessary to generate these features with anisotropic ice flow (Drews et al., 2013). Seismic reflections from within the ice rise indicate developed alignments of ice crystals (Hofstede et al., 2013). Radar data collected at three ice rises in the Fimbul Ice Shelf (Fig. 2) are being examined in terms of temporal changes in SMB patterns and differential variations of ice-shelf thicknesses adjacent to the ice rises.

Derwael Ice Rise deflects ice-shelf flow fed by West Ragnhild Glacier, one of the three largest glaciers in DML (Callens et al., 2014). The amplitudes of the observed Raymond arches fit best with models when it is assumed that the ice rise has been in a steady state or thinned slightly (~3 cm/a) over the past ~3.4 ka (Drews et al., 2015). The 120-m-long ice core drilled at the summit by the Belgian Antarctic Research Expeditions will constrain a climate record for the past century.

4.6. Other less-studied regions

The four regions described above constitute only about half of the Antarctic coast, and ice rises and rumples in the other half remain largely unexplored. Here, we review our knowledge of this unexplored region, moving eastward from DML.

There are fewer ice rises in Enderby Land (~50° E), Wilhelm II Land (~90° E), and Wilkes Land (~120° E) than in the above-mentioned regions, though there are many ice rumples in Wilheim II Land and Wilkes Land (Fig. 3). Here, ice-shelf extent is smaller than other regions in Antarctica, which partly explains the smaller population of isle-type ice rises. Only Mill Island (101° E) at the calving front of the Shackleton Ice Shelf and Law Dome (113° E) have been studied in these sectors. Inverse modeling using a 120-m-long borehole temperature profile acquired on Mill Island indicates surface temperature warming of 0.37° K per decade over the past 30 years (Roberts et al., 2013). The warming is attributed to changes in climate. The calving-front positions of many ice shelves in Wilkes Land, including Mill Island, changed synchronously, which suggests climate forcing (Miles et al., 2013). Law Dome is a

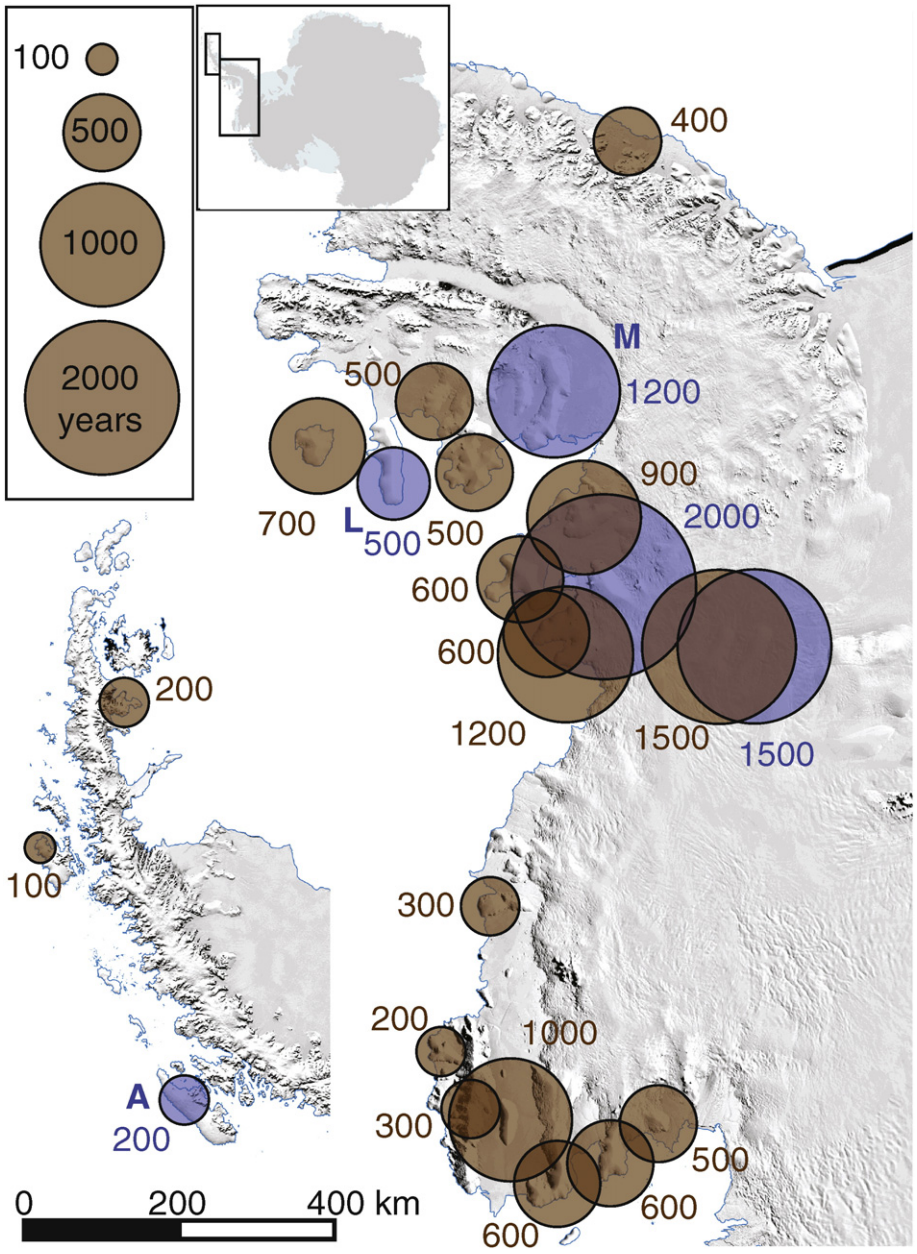

Fig. 10. Twenty three ice rises in the Antarctic Peninsula and Amundsen Sea coast that show a pair of distinct near-parallel lineations in satellite imagery in the central part of the ice rise (similar to those shown in Fig. 5). Inset shows the location. Numbers are the characteristic ice-flow time scale $T = (H/b$ in years, where H is ice thickness and b is SMB). The five ice rises shown with blue circles have well-developed, double-peaked Raymond arches (Fig. 9a); Adelaide Island (labeled as A), Latady Island (L) and Monteverdi Peninsula (M) were surveyed with ground-based radar and the other two with airborne radar. Background satellite image is Landsat (Bindschadler et al., 2008), and the calving front is highlighted in blue (Scientific Committee on Antarctic Research, 2012).

promontory-type ice rise with an independent flow center, and the saddle between this and the main ice sheet is the source of the Totten and Vanderford Glaciers. A full-depth (1196-m long) ice core was drilled near the summit of Law Dome and its high-resolution records have been used to determine past climate changes (e.g., Van Ommen et al., 2004). The stable isotope record near the bed indicates that Law Dome was not overridden by inland ice sheet during the LGM (Morgan et al., 1997). Geological evidence and GIA models suggest that Law Dome extended at least to the middle of the continental shelf, and probably to near the shelf break, 40–65 km away from the current ice margin, during the LGM and the adjacent ice sheet was a few hundred meters thicker than present (Goodwin and Zweck, 2000). The ice-core-derived SMB during the LGM was about one tenth of the present-day value, but this increased to the present-day value ~7 ka ago (Van Ommen et al., 2004). Published radargrams over the summit vicinity (Hamley et al., 1986) do not show Raymond arches, but the currently-available evidence is inadequate to confidently conclude their absence.

The Sulzberger Ice Shelf (150° E), east of the Ross Sea, has numerous ice rises and rumples (Fig. 3), but none have yet been studied. Upstream of this region (Marie Byrd Land) there are numerous rock outcrops that have been used to constrain ice extent during the LGM and the timing of Holocene deglaciation (Stone et al., 2003). Interpretations of such geological records in a regional perspective are subject to how far these ice rises affect the upstream region.

Some ice rises and rumples exist in Coats Land (~30° W) between the Ronne–Filchner Ice Shelf and DML. A much smaller ice-rise population in this region is distinct from the neighboring DML, even though they have similar ice-shelf extents and proximities of the calving front to the continental-shelf break. McDonald Ice Rumples (26° W) in the

Brunt Ice Shelf were first investigated by Limbert (1964) and Thomas (1971). They surveyed strain nets to determine the effect of the ice rumples on the flow of the ice shelf (Section 3).

5. Remaining challenges

Current understanding of ice rises and rumples is not sufficient to establish details of how they contribute to the dynamics and evolution of the Antarctic Ice Sheet. Below we list (not necessarily in order of importance) gaps in our understanding.

5.1 Net impact to ice-sheet and grounding-zone stability

Apart from the largest ice rises such as Roosevelt Island and Berkner Island, most ice rises and rumples are smaller than the grid size of continent-scale ice-sheet models (Table 1). Thus, their roles are only approximately evaluated in the context of continental or regional evolution. Although a prognostic model with sophisticated mechanics has been used to study stability effects (Favier et al., 2012), large-scale models using simpler mechanics (shallow-shelf approximations) are unlikely to be able to resolve the horizontal shear around small nascent ice rises. Further studies are needed to understand the consequences of the stabilizing effects of a grounded feature for regional ice-sheet/shelf evolution.

To resolve the dynamical effects of small features, model-grid size matters (e.g., Durand et al., 2009; Gladstone et al., 2012; Pattyn et al., 2012b). Studies using full-stress models with sub-grid resolution (2.5 km × 50 m) have shown that small-scale ice rises and rumples exert strong control on grounding-zone dynamics (e.g., Goldberg et al., 2009; Favier et al., 2012). To overcome the problem of scale and fully evaluate buttressing effects, others have started to include Schoof-type parameterizations of grounding-zone dynamics (Schoof, 2007; Schoof and Hindmarsh, 2010) in large-scale models as a means to better replicate observations (Gladstone et al., 2010; Pollard and DeConto, 2012). However, more observational data, including high-resolution bathymetry (Section 5.4) and terrestrial geological records from inland sites, are needed to further validate and develop both high-resolution numerical models and parameterizations of the effects of small-scale pinning points on grounding-zone dynamics.

Even less researched are possible destabilizing effects from ice rises and rumples (Section 2.6.4). The formation of tensile zones around ice rises and rumples (Fig. 2) reduces the drag they exert on the ice shelf. Moreover, weakening of shelves by crevassing likely increases calving, reducing the extent of the shelf and potentially reducing buttressing effects (Hulbe et al., 2010; Favier and Pattyn, 2015). Overall, it remains unclear whether the presence of ice rises can destabilize an ice shelf and grounding zone, and if so, what is the combination of conditions (e.g. location and distribution of ice rises, ice thickness, sea level) that might contribute to the destabilization?

5.2 Interactions with ocean and sea ice

Ocean circulation and basal melting of ice shelves may influence the presence, position, and shape of present-day ice rises, as well as their possible un-grounding in the future. The rapid retreat of Thwaites and Pine Island Glaciers was initiated by un-grounding of the ice shelf from an ice rumple near the grounding zone. Basal melting may have contributed to the un-grounding of Thwaites (Jenkins et al., 2010a; Tinto and Bell, 2011). Similar un-grounding likely happens elsewhere, but it remains unclear whether the presence of an ice rise or rumple would enhance or reduce basal melt by itself. Possible high melt may also influence ocean circulation, in addition to the effect of an elevated seabed around ice rises and rumples.

Coastal sea-ice distributions are affected by ice-shelf geometry and the presence of ice rises near the calving front (e.g., Tamura et al., 2008). The wind field modified by these obstacles often produces coastal polynyas to their west, and multi-year land-fast sea ice to their east (e.g., Massom et al., 2010). The former can increase sea-ice production, but such small changes are difficult to detect using satellite data. Also, it remains unknown how polynya's persistent presence and proximity to an ice shelf affect the production of continental-shelf water, the local ocean circulation and basal melting around nearby ice rises.

5.3 Equilibrium states and transitions between ice rises and rumples

We do not yet have sufficient knowledge of the geometries (e.g., ice draft, bathymetry) that allow ice rises, rumples, or non-grounded ice to exist in an equilibrium state (i.e., phase diagrams). Nor do we know details of how ice rises and rumples evolve. For example, what conditions can cause an ice rumple to transition to an ice rise, and what conditions can cause the transition from an ice rise to an ice rumple and/or to an ice shelf. Recent studies have suggested that ice rumples near Bungenstock Ice Rise (Fig. 1) may be decaying (Brunt et al., 2011) or growing (Bradley et al., 2015). Ongoing studies are needed to resolve these apparent inconsistencies.

Although the existence of many ice rises and rumples today suggests that they may be relatively stable features, numerical-model evidence is inadequate to show their stability. An elevated seabed is a necessary condition, but neither bed elevation nor ice thickness is sufficient to distinguish between ice rises and rumples (Table 1, Fig. 4). Further, the apparent hysteresis evident in the modeled evolution of ice rumples (Favier et al., 2012) suggests that non-linear interactions are important.

5.4 Bed topography and geology

Bathymetry on the continental shelves, especially beneath the ice shelves, is not sufficient to resolve small-scale seamounts that could be potential seeding sites for ice rises and rumples. Similarly, potential locations of ice rises and rumples during glacial periods are not resolved, which is consequential for the reconstruction of the expanded ice sheet during glacial periods. In order to determine whether the ice grounded there, past water depths need to be accurately modeled, and this necessitates the use of a coupled ice sheet-GIA model (Gomez et al., 2013; de Boer et al., 2014).

Many ice rises and rumples exist close to each other (Fig. 1). Does this mean that the conditions favorable to one are also favorable to the other, or does the presence of one produce favorable conditions for the other? Bed topography and relative positions of ice rises and rumples affect possible interactions within such clusters, which are difficult to investigate because of poorly resolved bathymetry. Similarly, do disappearing ice rises result in multiple, smaller grounded features that interact with each other and cause as-yet-undocumented complications? For example, many promontory-type ice rises have a local ice dome on the seaward side and a saddle towards the ice sheet. An ice rise at 24° E in DML has an elevated bed under the ice dome and a lowered bed under the saddle (Matsuoka et al., 2012; K. Matsuoka and F. Pattyn, unpublished data). When deglaciation occurs, this feature may separate into an isle-type ice rise seaward of a smaller promontory-type ice rise (Favier and Pattyn, 2015). A pair of such (possibly separated) ice rises is located at 16° E in DML.

The evolution of ice rises has been examined using radar-detected englacial stratigraphy and ice-flow models. For such modeling, radar-measured bed topography is available only beneath the grounded ice. Realistic bathymetry around the grounded ice is also needed to adequately model the grounding-zone position. Similarly, prognostic modeling of ice rises requires knowledge of the bed topography over the expanded extent of the ice rise. To determine bathymetry that can delineate seeding sites for ice rises and possible grounding-zone positions, vibroseismic measurements under ice shelves (Eisen et al., 2014) and multi-beam sonar soundings are necessary. Geological knowledge is also obtainable with these methods, and it is needed to evaluate basal stresses of the grounded features, especially when the

ice-bed interface is nearly thawed, which likely happens during the initial and terminal stages of an ice rise. It can also shed light on the seabed geology in areas that are otherwise more difficult to reach.

5.5 Ice core science: paleo-climate and chronology for ice-rise evolution

Stable ice rises are ideal sites to drill ice cores. The large SMB permits the retrieval of high-resolution temporal records over the past millennia. The International Partnership of Ice Core Science (IPICS) proposed ice cores that cover the past 2 ka and the entire LGM-Holocene transition and beyond (40-ka initiative). The relatively short characteristic times (Fig. 10) limit the range of the period covered by an ice-rise core, but most large ice rises are potential sites for the IPICS 2-ka initiative, and several are suitable for the IPICS 40-ka initiative (Mulvaney et al., 2007; Bertler et al., 2014; Mulvaney et al., 2014). Dense arrays of high temporal-resolution cores are needed to examine the spatial and temporal variability of atmospheric dynamics such as the El Nino-Southern Oscillation (e.g., Naik et al., 2010). The proximity of ice rises to the ocean makes them sensitive to regional climate and ocean variability.

Ice cores can help constrain the evolution of ice rises. For example, air trapped in bubbles in the ice can reveal histories of surface elevations and whether the ice rise is long-term emergent over a glacial-interglacial cycle. In addition, age-depth profiles from ice cores can be used to date radar-detected stratigraphy, which helps constrain the histories of climate and ice dynamics (Waddington et al., 2005).

5.6 Integrated science of inter-connected elements in Antarctica

Understanding the past, present and future of the Antarctic Ice Sheet requires a complete description of both the interior and coastal systems. The coastal system involves non-linear interactions between ice, ocean and the atmosphere. Although understanding of these interactions is improving, challenges still remain. A major challenge is that, although ice rises and rumples are small, their contributions to grounding-zone stability (instability) can be large. Because ephemerally grounded features provide little buttressing (Schmeltz et al., 2001), evolution of ice rises and rumples may have threshold-like impacts on ice-sheet dynamics as the shelf ice grounds and un-grounds. Uneven distribution of ice rises and rumples around Antarctica lead to different regional characteristics (Fig. 3). We do not know how much individual Antarctic regions contributed to rapid pulses of sea-level rise, such as MWP1a (Bentley et al., 2010, 2014; Weber et al., 2014). Exploring ice rises is a viable way to address the Holocene behavior of the ice sheet at a high temporal resolution. To decipher the evolution of the Antarctic Ice Sheet, we first need to describe the system science in the coastal region.

Acknowledgments

This manuscript is an outcome of an International Workshop on Antarctic Ice Rises held at the Norwegian Polar Institute (NPI) in Tromsø, 2013. We acknowledge sponsors of this workshop: Standing Science Group on Physical Sciences of the Scientific Committee on Antarctic Research (SCAR), World Climate Research Programme's Climate and Cryosphere (CliC) project, Association of Polar Early Career Scientists (APECS), Research Council of Norway's MILUTV-ARENAER program, British Antarctic Survey, and NPI's Center for Ice, Climate, and Ecosystems. Fig. 2 was constructed by Audun Igesund of NPI and Fig. 7 by Chris Orton of Durham University. Maps in this paper (Figs. 1, 3, 5, 6 and 10) were prepared using Quantarctica (www.quantarctica.org). Workshop outcomes, such as talk slides and video, posters, and short video clips (FrostBytes) introducing poster presentations for non specialists are hosted by CliC and available at http://www.climate-cryosphere.org/meetings/past/2013/ice-rises-2013.

Appendix A. Inventory of ice rises and rumples

The inventory is based on available grounding-zone products and some additional visual interpretation of satellite imagery. Beginning with the island polygons of the MODIS Mosaic of Antarctica (MOA) 2003–2004 product (Haran et al., 2005; Scambos et al., 2007), we extracted all island polygons that were contained within an ice shelf, assuming that they represent ice rises or rumples. We then updated this dataset using the new MOA 2009 product as well as independent grounding-zone points from SAR interferometry (Rignot et al., 2011b) and ICESat altimetry (Fricker et al., 2009; Brunt et al., 2010). This preliminary inventory was then manually edited and updated based on visual interpretation of the two MOA image mosaics, the high-resolution Landsat Image Mosaic of Antarctica (LIMA) (Bindschadler et al., 2008), and the IPY-MEaSUREs Antarctica velocity map (Rignot et al., 2011a). We also digitized polygons around the most prominent ice ridges and domes within the continental grounding zone.

The grounded features fall into four groups. The first group is identified by clearly elevated features that are very likely isle-type ice rises surrounded by ice shelves and is labeled 'identifier 1' in the inventory and Table 1. The second group is identified by prominent ice ridges and domes connected to the inland ice sheet (promontory-type ice rises, 'identifier 2'). Their landward extent is often hard to discern. We do not use a clear criterion to include or not such features in this inventory; the inventoried features are samples that either have been investigated or could be interesting research targets. The third group is identified by less-prominent grounded isles that show more diffuse, dynamic characteristics. Such features include ice rumples ('identifier 3'). The fourth group is similar to the first group but features have outcropping bedrock or sediments (Scientific Committee on Antarctic Research, 2012) within the grounded features ('identifier 4').

Attributes of individual features are provided in the inventory and associated population statistics are presented in Table 1 and Fig. 4, which are discussed in Section 2.4. These attributes include: maximum, minimum and mean values of bed elevations and ice-surface elevations, maximum ice thickness, mean ice-surface slope, relative height of the highest place (summit) of the feature measured from the adjacent ice shelf or stream surface (all data are from the Bedmap2 dataset (Fretwell et al., 2013)), and mean ice-flow speed (Rignot et al., 2011a). These datasets have grid sizes of 1 km, so may include large errors associated with the spatial extent of the grounded features. Elevations are referenced to the GL04C geoid, which is used for the Bedmap2 dataset (Fretwell et al., 2013).

This inventory is aimed to provide an approximate picture of their continent-wide distribution and overall characteristics; there are likely many undetected features. The inventory is provided through a data center at the Norwegian Polar Institute: data.npolar.no/dataset/9174e644-3540-44e8-b00b-c629acbf1339. We provide this inventory in a shape file format with an associated GIS style file that enable use of the inventory as part of free-GIS data package "Quantarctica" downloadable at www.quantarctica.org.

References

Anderson, J.B., 1999. Antarctic Marine Geology. Cambridge University Press, Cambridge.
Anderson, J.B., Conway, H., Bart, P.J., Witus, A.E., Greenwood, S.L., McKay, R.M., Hall, B.L., Ackert, R.P., Licht, K., Jakobsson, M., Stone, J.O., 2014. Ross Sea paleo-ice sheet drainage and deglacial history during and since the LGM. Quat. Sci. Rev. 100, 31–54. http://dx.doi.org/10.1016/j.quascirev.2013.08.020.
Arndt, J.E., Schenke, H.W., Jakobsson, M., Nitsche, F.O., Buys, G., Goleby, B., Rebesco, M., Bohoyo, F., Hong, J., Black, J., Greku, R., Udintsev, G., Barrios, F., Reynoso-Peralta, W., Taisei, M., Wigley, R., 2013. The International Bathymetric Chart of the Southern Ocean (IBCSO) version 1.0 — A new bathymetric compilation covering circum-Antarctic waters. Geophys. Res. Lett. 40, 3111–3117. http://dx.doi.org/10.1002/grl.50413.
Arthern, R.J., Winebrenner, D.P., Vaughan, D.G., 2006. Antarctic snow accumulation mapped using polarization of 4.3-cm wavelength microwave emission. J. Geophys. Res.-Atmos. 111 (D6), D06107. http://dx.doi.org/10.1029/2004JD005667.

Årthun, M., Nicholls, K.W., Boehme, L., 2013. Wintertime Water Mass Modification near an Antarctic Ice Front. J. Phys. Oceanogr. 43 (2), 359–365. http://dx.doi.org/10.1175/jpo-d-12-0186.1.

Årthun, M., Nicholls, K.W., Makinson, K., Fedak, M.A., Boehme, L., 2012. Seasonal inflow of warm water onto the southern Weddell Sea continental shelf, Antarctica. Geophys. Res. Lett. 39 (17), L17601. http://dx.doi.org/10.1029/2012gl052856.

Balco, G., Schaefer, J.M., 2013. Exposure-age record of Holocene ice sheet and ice shelf change in the northeast Antarctic Peninsula. Quat. Sci. Rev. 59, 101–111. http://dx.doi.org/10.1016/j.quascirev.2012.10.022.

Bamber, J.L., Gomez-Dans, J.L., Griggs, J.A., 2009. A new 1 km digital elevation model of the Antarctic derived from combined satellite radar and laser data, - Part 1: Data and methods. Cryosphere 3 (1), 101–111. http://dx.doi.org/10.5194/tc-3-101-2009.

Bentley, M.J., Cofaigh, C.O., Anderson, J.B., Conway, H., Davies, B., Graham, A.G.C., Hillenbrand, C.-D., Hodgson, D.A., Jamieson, S.S.R., Larter, R.D., Mackintosh, A., Smith, J.A., Verleyen, E., Ackert, R.P., Bart, P.J., Berg, S., Brunstein, D., Canals, M., Colhoun, E.A., Crosta, X., Dickens, W.A., Domack, E., Dowdeswell, J.A., Dunbar, R., Ehrmann, W., Evans, J., Favier, V., Fink, D., Fogwill, C.J., Glasser, N.F., Gohl, K., Golledge, N.R., Goodwin, I., Gore, D.B., Greenwood, S.L., Hall, B.L., Hall, K., Hedding, D.W., Hein, A.S., Hocking, E.P., Jakobsson, M., Johnson, J.S., Jomelli, V., Jones, R.S., Klages, J.P., Kristoffersen, Y., Kuhn, G., Leventer, A., Licht, K., Lilly, K., Lindow, J., Livingstone, S.J., Masse, G., McGlone, M.S., McKay, R.M., Melles, M., Miura, H., Mulvaney, R., Nel, W., Nitsche, F.O., O'Brien, P.E., Post, A.L., Roberts, S.J., Saunders, K.M., Selkirk, P.M., Simms, A.R., Spiegel, C., Stolldorf, T.D., Sugden, D.E., van der Putten, N., van Ommen, T., Verfaillie, D., Vyverman, W., Wagner, B., White, D.A., Witus, A.E., Zwartz, D., Consortium, R., 2014. A community-based geological reconstruction of Antarctic Ice Sheet deglaciation since the Last Glacial Maximum. Quat. Sci. Rev. 100, 1–9. http://dx.doi.org/10.1016/j.quascirev.2014.06.025.

Bentley, M.J., Fogwill, C.J., Le Brocq, A.M., Hubbard, A.L., Sugden, D.E., Dunai, T.J., Freeman, S.P.H.T., 2010. Deglacial history of the West Antarctic Ice Sheet in the Weddell Sea embayment: Constraints on past ice volume change. Geology 38 (5), 411–414. http://dx.doi.org/10.1130/g30754.1.

Bertler, N., Conway, H., Dahl-Jensen, D., Blunier, T., Brook, E., Dadic, R., Delmonte, B., Dongqi, Z., Edwards, R., Emanuelsson, D., Fudge, T., Golledge, N., Hindmarsh, R., Hawley, R., Kipfstuhl, S., Kjaer, H., Kurbatov, A., Lee, J., Mayewski, P.A., Naish, T., Neff, P., Scherer, R., Severinghaus, J., Simonsen, M., Steig, E.J., Tuohy, A., Vallenlonga, P., Waddington, E.D., 2014. The Roosevelt Island Climate Evolution (RICE) project — Did the Ross Ice Shelf Collapse During MIS 5e?, AGU Fall Meeting. AGU, San Francisco.

Bindschadler, R., 1993. Siple Coast Project research of Crary Ice Rise and the mouths of Ice Streams B and C, West Antarctica: review and new perspectives. J. Glaciol. 39 (133), 538–552.

Bindschadler, R., Choi, H., Wichlacz, A., Bingham, R., Bohlander, J., Brunt, K., Corr, H., Drews, R., Fricker, H., Hall, M., Hindmarsh, R., Kohler, J., Padman, L., Rack, W., Rotschky, G., Urbini, S., Vornberger, P., Young, N., 2011. Getting around Antarctica: new high-resolution mappings of the grounded and freely-floating boundaries of the Antarctic ice sheet created for the International Polar Year. Cryosphere 5 (3), 569–588. http://dx.doi.org/10.5194/tc-5-569-2011.

Bindschadler, R., Roberts, E.P., Iken, A., 1990. Age of Crary Ice Rise, Antarctica, determined from temperature-depth profiles. Ann. Glaciol. 14 (1), 13–16.

Bindschadler, R., Vornberger, P., Fleming, A., Fox, A., Mullins, J., Binnie, D., Paulsen, S.J., Granneman, B., Gorodetzky, D., 2008. The Landsat Image Mosaic of Antarctica. Remote Sens. Environ. 112 (12), 4214–4226. http://dx.doi.org/10.1016/j.rse.2008.07.006.

Bindschadler, R.A., Roberts, E.P., Macayeal, D.R., 1989. Distribution of net mass balance in the vicinity of Crary Ice Rise, Antarctica. J. Glaciol. 35 (121), 370–377.

Blindow, N., Suckro, S.K., Rueckamp, M., Braun, M., Schindler, M., Breuer, B., Saurer, H., Simoes, J.C., Lange, M.A., 2010. Geometry and thermal regime of the King George Island ice cap, Antarctica, from GPR and GPS. Ann. Glaciol. 51 (55), 103–109. http://dx.doi.org/10.3189/172756410791392691.

de Boer, B., Stocchi, P., van de Wal, R.S.W., 2014. A fully coupled 3-D ice-sheet-sea-level model: algorithm and applications. Geosci. Model Dev. 7 (5), 2141–2156. http://dx.doi.org/10.5194/gmd-7-2141-2014.

Borstad, C.P., Rignot, E., Mouginot, J., Schodlok, M.P., 2013. Creep deformation and buttressing capacity of damaged ice shelves: theory and application to Larsen C ice shelf. Cryosphere 7 (6), 1931–1947. http://dx.doi.org/10.5194/tc-7-1931-2013.

Bradley, S.L., Hindmarsh, R.C.A., Whitehouse, P.L., Bentley, M.J., King, M.A., 2015. Low post-glacial rebound rates in the Weddell Sea due to Late Holocene ice-sheet readvance. Earth Planet. Sci. Lett. 413, 79–89. http://dx.doi.org/10.1016/j.epsl.2014.12.039.

Braun, M., Humbert, A., Moll, A., 2009. Changes of Wilkins Ice Shelf over the past 15 years and inferences on its stability. Cryosphere 3 (1), 41–56. http://dx.doi.org/10.5194/tc-3-41-2009.

van den Broeke, M., van de Berg, W.J., van Meijgaard, E., 2006. Snowfall in coastal West Antarctica much greater than previously assumed. Geophys. Res. Lett. 33 (2), L02505.

Brook, E.J., White, J.W.C., Schilla, A.S.M., Bender, M.L., Barnett, B., Severinghaus, J.P., Taylor, K.C., Alley, R.B., Steig, E.J., 2005. Timing of millennial-scale climate change at Siple Dome, West Antarctica, during the last glacial period. Quat. Sci. Rev. 24 (12–13), 1333–1343. http://dx.doi.org/10.1016/j.quascirev.2005.02.002.

Brunt, K.M., Fricker, H.A., Padman, L., 2011. Analysis of ice plains of the Filchner–Ronne Ice Shelf, Antarctica, using ICESat laser altimetry. J. Glaciol. 57 (205), 965–975. http://dx.doi.org/10.3189/002214311798043753.

Brunt, K.M., Fricker, H.A., Padman, L., Scambos, T.A., O'Neel, S., 2010. Mapping the grounding zone of the Ross Ice Shelf, Antarctica, using ICESat laser altimetry. Ann. Glaciol. 51 (55), 71–79. http://dx.doi.org/10.3189/172756410791392790.

Callens, D., Matsuoka, K., Steinhage, D., Smith, B., Witrant, E., Pattyn, F., 2014. Transition of flow regime along a marine-terminating outlet glacier in East Antarctica. Cryosphere 8 (3), 867–875. http://dx.doi.org/10.5194/tc-8-867-2014.

Catania, G., Hulbe, C., Conway, H., 2010. Grounding-line basal melt rates determined using radar-derived internal stratigraphy. J. Glaciol. 56 (197), 545–554. http://dx.doi.org/10.3189/002214310792447842.

Catania, G., Hulbe, C., Conway, H., Scambos, T.A., Raymond, C.F., 2012. Variability in the mass flux of the Ross ice streams, West Antarctica, over the last millennium. J. Glaciol. 58 (210), 741–752. http://dx.doi.org/10.3189/2012JoG11J219.

Chavanne, C.P., Heywood, K.J., Nicholls, K.W., Fer, I., 2010. Observations of the Antarctic Slope Undercurrent in the southeastern Weddell Sea. Geophys. Res. Lett. 37 (13), L13601. http://dx.doi.org/10.1029/2010gl043603.

Conway, H., Catania, G., Conway, M., Rasmussen, L.A., Raymond, C.F., Marshall, H.P., O'Neel, S., 2005. Glacial history of the ridge between Mercer and van der Veen Ice Streams. 12th Annual WAIS Workshop, Sterling, VA.

Conway, H., Hall, B.L., Denton, G.H., Gades, A.M., Waddington, E.D., 1999. Past and future grounding-line retreat of the West Antarctic Ice Sheet. Science 286 (5438), 280–283. http://dx.doi.org/10.1126/science.286.5438.280.

Cook, A.J., Vaughan, D.G., 2010. Overview of areal changes of the ice shelves on the Antarctic Peninsula over the past 50 years. Cryosphere 4 (1), 77–98. http://dx.doi.org/10.5194/tc-4-77-2010.

Craven, M., Allison, I., Fricker, H.A., Warner, R., 2009. Properties of a marine ice layer under the Amery Ice Shelf, East Antarctica. J. Glaciol. 55 (192), 717–728. http://dx.doi.org/10.3189/002214309789470941.

Cuffey, K.M., Paterson, W.S.B., 2010. The Physics of Glaciers. Academic Press.

De Rydt, J., Holland, P.R., Dutrieux, P., Jenkins, A., 2014. Geometric and oceanographic controls on melting beneath Pine Island Glacier. J. Geophys. Res. Oceans 119 (4), 2420–2438. http://dx.doi.org/10.1002/2013jc009513.

Depoorter, M.A., Bamber, J.L., Griggs, J.A., Lenaerts, J.T.M., Ligtenberg, S.R.M., van den Broeke, M.R., Moholdt, G., 2013. Calving fluxes and basal melt rates of Antarctic ice shelves. Nature 502 (7469), 89–93. http://dx.doi.org/10.1038/nature12567.

Dinniman, M.S., Klinck, J.M., Hofmann, E.E., 2012. Sensitivity of circumpolar deep water transport and ice shelf basal melt along the West Antarctic Peninsula to changes in the winds. J. Clim. 25 (14), 4799–4816. http://dx.doi.org/10.1175/jcli-d-11-00307.1.

Doake, C.S.M., Corr, H.F.J., Rott, H., Skvarca, P., Young, N.W., 1998. Breakup and conditions for stability of the northern Larsen Ice Shelf, Antarctica. Nature 391 (6669), 778–780. http://dx.doi.org/10.1038/35832.

Drews, R., Martín, C., Steinhage, D., Eisen, O., 2013. Characterizing the glaciological conditions at Halvfarryggen ice dome, Dronning Maud Land, Antarctica. J. Glaciol. 59 (213), 9–20. http://dx.doi.org/10.3189/2013JoG12J134.

Drews, R., Matsuoka, K., Martín, C., Callens, D., Bergeot, N., Pattyn, F., 2015. Evolution of Derwael Ice Rise in Dronning Maud Land, Antarctica, over the last millennia. J. Geophys. Res. Earth Surf. 120 (3), 564–579. http://dx.doi.org/10.1002/2014JF003246.

Durand, G., Gagliardini, O., de Fleurian, B., Zwinger, T., Le Meur, E., 2009. Marine ice sheet dynamics: Hysteresis and neutral equilibrium. J. Geophys. Res. Earth Surf. 114 (F3), F03009. http://dx.doi.org/10.1029/2008JF001170.

Eisen, O., Hofstede, C., Diez, A., Kristoffersen, Y., Lambrecht, A., Mayer, C., Blenkner, R., Hilmarsson, S., 2014. On-ice vibroseis and snowstreamer systems for geoscientific research. Polar Sci. 9 (1), 51–65. http://dx.doi.org/10.1016/j.polar.2014.10.003.

Fahnestock, M.A., Scambos, T.A., Bindschadler, R.A., Kvaran, G., 2000. A millennium of variable ice flow recorded by the Ross Ice Shelf, Antarctica. J. Glaciol. 46 (155), 652–664. http://dx.doi.org/10.3189/172756500781832693.

Farrell, W.E., Clark, J.A., 1976. On postglacial sea level. Geophys. J. R. Astron. Soc. 46 (3), 647–667. http://dx.doi.org/10.1111/j.1365-246X.1976.tb01252.x.

Favier, L., Pattyn, F., 2015. Antarctic ice-rise formation, evolution and stability. Geophys. Res. Lett. 42 (11), 4456–4463. http://dx.doi.org/10.1002/2015gl064195.

Favier, L., Gagliardini, O., Durand, G., Zwinger, T., 2012. A three-dimensional full Stokes model of the grounding line dynamics: effect of a pinning point beneath the ice shelf. Cryosphere 6 (1), 101–112. http://dx.doi.org/10.5194/tc-6-101-2012.

Fernandoy, F., Meyer, H., Oerter, H., Wilhelms, F., Graf, W., Schwander, J., 2010. Temporal and spatial variation of stable-isotope ratios and accumulation rates in the hinterland of Neumayer station, East Antarctica. J. Glaciol. 56 (198), 673–687. http://dx.doi.org/10.3189/002214310793146296.

Fowler, A.C., 1992. Modelling ice sheet dynamics. Geophys. Astrophys. Fluid Dyn. 63 (1–4), 29–65. http://dx.doi.org/10.1080/03091929208228277.

Fretwell, P., Pritchard, H.D., Vaughan, D.G., Bamber, J.L., Barrand, N.E., Bell, R., Bianchi, C., Bingham, R.G., Blankenship, D.D., Casassa, G., Catania, G., Callens, D., Conway, H., Cook, A.J., Corr, H.F.J., Damaske, D., Damm, V., Ferraccioli, F., Forsberg, R., Fujita, S., Gim, Y., Gogineni, P., Griggs, J.A., Hindmarsh, R.C.A., Holmlund, P., Holt, J.W., Jacobel, R.W., Jenkins, A., Jokat, W., Jordan, T., King, E.C., Kohler, J., Krabill, W., Riger-Kusk, M., Langley, K.A., Leitchenkov, G., Leuschen, C., Luyendyk, B.P., Matsuoka, K., Mouginot, J., Nitsche, F.O., Nogi, Y., Nost, O.A., Popov, S.V., Rignot, E., Rippin, D.M., Rivera, A., Roberts, J., Ross, N., Siegert, M.J., Smith, A.M., Steinhage, D., Studinger, M., Sun, B., Tinto, B.K., Welch, B.C., Wilson, D., Young, D.A., Xiangbin, C., Zirizzotti, A., 2013. Bedmap2: improved ice bed, surface and thickness datasets for Antarctica. Cryosphere 7 (1), 375–393. http://dx.doi.org/10.5194/tc-7-375-2013.

Fricker, H.A., Padman, L., 2006. Ice shelf grounding zone structure from ICESat laser altimetry. Geophys. Res. Lett. 33 (15), L15502. http://dx.doi.org/10.1029/2006GL026907.

Fricker, H.A., Coleman, R., Padman, L., Scambos, T.A., Bohlander, J., Brunt, K.M., 2009. Mapping the grounding zone of the Amery Ice Shelf, East Antarctica using InSAR, MODIS and ICESat. Antarct. Sci. 21 (5), 515–532. http://dx.doi.org/10.1017/s095410200999023x.

Fricker, H.A., Popov, S., Allison, I., Young, N., 2001. Distribution of marine ice beneath the Amery Ice Shelf. Geophys. Res. Lett. 28 (11), 2241–2244. http://dx.doi.org/10.1029/2000gl012461.

Fujita, S., Holmlund, P., Matsuoka, K., Enomoto, H., Fukui, K., Nakazawa, F., Sugiyama, S., Surdyk, S., 2012. Radar diagnosis of the subglacial conditions in Dronning Maud

Land, East Antarctica. Cryosphere 6 (5), 1203–1219. http://dx.doi.org/10.5194/tc-6-1203-2012.
Fürst, J.J., Durand, G., Gillet-Chaulet, F., Merino, N., Tavard, L., Mouginot, J., Gourmelen, N., Gagliardini, O., 2015. Assimilation of Antarctic velocity observations provides evidence for uncharted pinning points. Cryosphere 9, 1427–1443. http://dx.doi.org/10.5194/tcd-9-1461-2015.
Gagliardini, O., Durand, G., Zwinger, T., Hindmarsh, R.C.A., Le Meur, E., 2010. Coupling of ice-shelf melting and buttressing is a key process in ice-sheets dynamics. Geophys. Res. Lett. 37 (14), L14501. http://dx.doi.org/10.1029/2010GL043334.
Gillet-Chaulet, F., Hindmarsh, R.C.A., Corr, H.F.J., King, E.C., Jenkins, A., 2011. In-situ quantification of ice rheology and direct measurement of the Raymond Effect at Summit, Greenland using a phase-sensitive radar. Geophys. Res. Lett. 38 (24), L24503. http://dx.doi.org/10.1029/2011GL049843.
Gladish, C.V., Holland, D.M., Holland, P.R., Price, S.F., 2012. Ice-shelf basal channels in a coupled ice/ocean model. J. Glaciol. 58 (212), 1227–1244. http://dx.doi.org/10.3189/2012JoG12J003.
Gladstone, R.M., Lee, V., Rougier, J., Payne, A.J., Hellmer, H., Le Brocq, A., Shepherd, A., Edwards, T.L., Gregory, J., Cornford, S.L., 2012. Calibrated prediction of Pine Island Glacier retreat during the 21st and 22nd centuries with a coupled flowline model. Earth Planet. Sci. Lett. 333-334, 191–199. http://dx.doi.org/10.1016/j.epsl.2012.04.022.
Gladstone, R.M., Lee, V., Vieli, A., Payne, A.J., 2010. Grounding line migration in an adaptive mesh ice sheet model. J. Geophys. Res. Earth Surf. 115 (F4), F04014. http://dx.doi.org/10.1029/2009JF001615.
Glasser, N.F., Gudmundsson, G.H., 2012. Longitudinal surface structures (flowstripes) on Antarctic glaciers. Cryosphere 6 (2), 383–391. http://dx.doi.org/10.5194/tc-6-383-2012.
Glasser, N.F., Kulessa, B., Luckman, A., Jansen, D., King, E.C., Sammonds, P.R., Scambos, T.A., Jezek, K.C., 2009. Surface structure and stability of the Larsen C ice shelf, Antarctic Peninsula. J. Glaciol. 55 (191), 400–410. http://dx.doi.org/10.3189/002214309788816597.
Goldberg, D., Holland, D.M., Schoof, C., 2009. Grounding line movement and ice shelf buttressing in marine ice sheets. J. Geophys. Res. Earth Surf. 114 (F4), F04026. http://dx.doi.org/10.1029/2008JF001227.
Gomez, N., Pollard, D., Mitrovica, J.X., 2013. A 3-D coupled ice sheet - sea level model applied to Antarctica through the last 40 ky. Earth Planet. Sci. Lett. 384, 88–99. http://dx.doi.org/10.1016/j.epsl.2013.09.042.
Goodwin, A.H., Vaughan, D.G., 1995. A topographic origin for double-ridge features in visible imagery of ice divides in Antarctica. J. Glaciol. 41 (139), 483–489.
Goodwin, I.D., Zweck, C., 2000. Glacio-isostasy and glacial ice load at Law Dome, Wilkes Land, East Antarctica. Quat. Res. 53 (3), 285–293. http://dx.doi.org/10.1006/qres.1999.2125.
Goodwin, I.D., Browning, S., Lorrey, A.M., Mayewski, P.A., Phipps, S.J., Bertler, N.A.N., Edwards, R.P., Cohen, T.J., van Ommen, T., Curran, M., Barr, C., Stager, J.C., 2014. A reconstruction of extratropical Indo-Pacific sea-level pressure patterns during the Medieval Climate Anomaly. Clim. Dyn. 43 (5–6), 1197–1219. http://dx.doi.org/10.1007/s00382-013-1899-1.
Gorodetskaya, I.V., Van Lipzig, N.P.M., Van den Broeke, M.R., Mangold, A., Boot, W., Reijmer, C.H., 2013. Meteorological regimes and accumulation patterns at Utsteinen, Dronning Maud Land, East Antarctica: analysis of two contrasting years. J. Geophys. Res.-Atmos. 118 (4), 1700–1715. http://dx.doi.org/10.1002/jgrd.50177.
Gudmundsson, G.H., 2003. Transmission of basal variability to a glacier surface. J. Geophys. Res. Solid Earth 108 (B5), 2253. http://dx.doi.org/10.1029/2002jb002107.
Hamley, T.C., Morgan, V.I., Thwaites, R.J., 1986. An ice-core drilling site at Law Dome summit, Wilkes Land, Antartica. ANARE Research Notes, 37.
Haran, T.M., Bohlander, J., Scambos, T., Fahnestock, M., 2005. MODIS Mosaic of Antarctica (MOA) Image Map. National Snow and Ice Data Center http://dx.doi.org/10.7265/N5ZK5DM5.
Hattermann, T., Nøst, O.A., Lilly, J.M., Smedsrud, L.H., 2012. Two years of oceanic observations below the Fimbul Ice Shelf, Antartica. Geophys. Res. Lett. 39 (12), L12605. http://dx.doi.org/10.1029/2012gl051012.
Hattermann, T., Smedsrud, L.H., Nost, O.A., Lilly, J.M., Galton-Fenzi, B.K., 2014. Eddy-resolving simulations of the Fimbul Ice Shelf cavity circulation: Basal melting and exchange with open ocean. Ocean Model. 82, 28–44. http://dx.doi.org/10.1016/j.ocemod.2014.07.004.
Hellmer, H.H., Jacobs, S.S., 1992. Ocean interactions with the base of Amery Ice Shelf, Antarctica. J. Geophys. Res. Oceans 97 (C12), 20305–20317. http://dx.doi.org/10.1029/92jc01856.
Hellmer, H.H., Kauker, F., Timmermann, R., Determann, J., Rae, J., 2012. Twenty-first-century warming of a large Antarctic ice-shelf cavity by a redirected coastal current. Nature 485 (7397), 225–228. http://dx.doi.org/10.1038/nature11064.
Helm, V., Humbert, A., Miller, H., 2014. Elevation and elevation change of Greenland and Antarctica derived from CryoSat-2. Cryosphere 8 (4), 1539–1559. http://dx.doi.org/10.5194/tc-8-1539-2014.
Heroy, D.C., Anderson, J.B., 2007. Radiocarbon constraints on Antarctic Peninsula Ice Sheet retreat following the Last Glacial Maximum (LGM). Quat. Sci. Rev. 26 (25–28), 3286–3297. http://dx.doi.org/10.1016/j.quascirev.2007.07.012.
Hillenbrand, C.-D., Bentley, M.J., Stolldorf, T.D., Hein, A.S., Kuhn, G., Graham, A.G.C., Fogwill, C.J., Kristoffersen, Y., Smith, J.A., Anderson, J.B., Larter, R.D., Melles, M., Hodgson, D.A., Mulvaney, R., Sugden, D.E., 2013. Reconstruction of changes in the Weddell Sea sector of the Antarctic Ice Sheet since the Last Glacial Maximum. Quat. Sci. Rev. 100, 111–136. http://dx.doi.org/10.1016/j.quascirev.2013.07.020.
Hindmarsh, R.C.A., 1996. Stochastic perturbation of divide position. Ann. Glaciol. 23, 94–104.
Hindmarsh, R.C.A., King, E.C., Mulvaney, R., Corr, H.F.J., Hiess, G., Gillet-Chaulet, F., 2011. Flow at ice-divide triple junctions: 2. Three-dimensional views of isochrone architecture from ice-penetrating radar surveys. J. Geophys. Res. Earth Surf. 116 (F2), F02024. http://dx.doi.org/10.1029/2009jf001622.
Hofstede, C., Eisen, O., Diez, A., Jansen, D., Kristoffersen, Y., Lambrecht, A., Mayer, C., 2013. Investigating englacial reflections with vibro- and explosive-seismic surveys at Halvfarryggen ice dome, Antarctica. Ann. Glaciol. 54 (64), 189–200. http://dx.doi.org/10.3189/2013AoG64A064.
Holland, D.M., Jenkins, A., 1999. Modeling thermodynamic ice–ocean interactions at the base of an ice shelf. J. Phys. Oceanogr. 29 (8), 1787–1800. http://dx.doi.org/10.1175/1520-0485(1999)029<1787:mtioia>2.0.co;2.
Holland, P.R., Corr, H.F.J., Vaughan, D.G., Jenkins, A., Skvarca, P., 2009. Marine ice in Larsen Ice Shelf. Geophys. Res. Lett. 36 (11), L11604. http://dx.doi.org/10.1029/2009gl038162.
Horgan, H.J., Anandakrishnan, S., 2006. Static grounding lines and dynamic ice streams: Evidence from the Siple Coast, West Antarctica. Geophys. Res. Lett. 33 (18), L18502. http://dx.doi.org/10.1029/2006gl027091.
Hughes, T., 1973. Is the west Antarctic Ice Sheet disintegrating? J. Geophys. Res. 78 (33), 7884–7910. http://dx.doi.org/10.1029/JC078i033p07884.
Hulbe, C., Fahnestock, M., 2007. Century-scale discharge stagnation and reactivation of the Ross ice streams, West Antarctica. J. Geophys. Res. Earth Surf. 112 (F3), F03S27. http://dx.doi.org/10.1029/2006jf000603.
Hulbe, C.L., LeDoux, C., Cruikshank, K., 2010. Propagation of long fractures in the Ronne Ice Shelf, Antarctica, investigated using a numerical model of fracture propagation. J. Glaciol. 56 (197), 459–472. http://dx.doi.org/10.3189/002214310792447743.
Humbert, A., Steinhage, D., 2011. The evolution of the western rift area of the Fimbul Ice Shelf, Antarctica. Cryosphere 5 (4), 931–944. http://dx.doi.org/10.5194/tc-5-931-2011.
Hvidberg, C.S., 1996. Steady-state thermomechanical modelling of ice flow near the center of large ice sheets with the finite-element technique. Ann. Glaciol. 23, 116–123.
Jacobs, S.S., Comiso, J.C., 1989. Sea ice and oceanic processes on the Ross Sea continental shelf. J. Geophys. Res. Oceans 94 (C12), 18195–18211. http://dx.doi.org/10.1029/JC094iC12p18195.
Jacobs, S.S., Helmer, H.H., Doake, C.S.M., Jenkins, A., Frolich, R.M., 1992. Melting of ice shelves and the mass balance of Antarctica. J. Glaciol. 38 (130), 375–387.
Jacobs, S.S., Jenkins, A., Giulivi, C.F., Dutrieux, P., 2011. Stronger ocean circulation and increased melting under Pine Island Glacier ice shelf. Nat. Geosci. 4 (8), 519–523. http://dx.doi.org/10.1038/ngeo1188.
Jacobson, H.P., Waddington, E.D., 2004. Recumbent folding in ice sheets: a core-referential study. J. Glaciol. 50 (168), 3–16. http://dx.doi.org/10.3189/172756504781830204.
Jansen, D., Luckman, A., Kulessa, B., Holland, P.R., King, E.C., 2013. Marine ice formation in a suture zone on the Larsen C Ice Shelf and its influence on ice shelf dynamics. J. Geophys. Res. Earth Surf. 118 (3), 1628–1640. http://dx.doi.org/10.1002/jgrf.20120.
Jenkins, A., Dutrieux, P., Jacobs, S.S., McPhail, S.D., Perrett, J.R., Webb, A.T., White, D., 2010a. Observations beneath Pine Island Glacier in West Antarctica and implications for its retreat. Nat. Geosci. 3 (7), 468–472. http://dx.doi.org/10.1038/ngeo890.
Jenkins, A., Nicholls, K.W., Corr, H.F.J., 2010b. Observation and parameterization of ablation at the base of Ronne Ice Shelf, Antarctica. J. Phys. Oceanogr. 40 (10), 2298–2312. http://dx.doi.org/10.1175/2010jpo4317.1.
Jezek, K.C., 1984. A modified theory of bottom crevasses used as a means for measuring the buttressing effect of ice shelves on inland ice sheets. J. Geophys. Res. Solid Earth 89 (B3), 1925–1931. http://dx.doi.org/10.1029/JB089iB03p01925.
Jezek, K.C., RAMP Product Team, 2002. RAMP AMM-1 SAR Image Mosaic of Antarctica. Version 2. http://dx.doi.org/10.5067/8AF4ZRPULS4H.
Joughin, I., Padman, L., 2003. Melting and freezing beneath Filchner–Ronne Ice Shelf, Antarctica. Geophys. Res. Lett. 30 (9), 1477. http://dx.doi.org/10.1029/2003gl016941.
Joughin, I., Smith, B.E., Medley, B., 2014. Marine ice sheet collapse potentially under way for the Thwaites Glacier Basin, West Antarctica. Science 344 (6185), 735–738. http://dx.doi.org/10.1126/science.1249055.
Khazendar, A., Tison, J.L., Stenni, B., Dini, M., Bondesan, A., 2001. Significant marine-ice accumulation in the ablation zone beneath an Antarctic ice shelf. J. Glaciol. 47 (158), 359–368. http://dx.doi.org/10.3189/172756501781832160.
Kim, K.T., Jezek, K.C., Sohn, H.G., 2001. Ice shelf advance and retreat rates along the coast of Queen Maud Land, Antarctica. J. Geophys. Res. Oceans 106 (C4), 7097–7106. http://dx.doi.org/10.1029/2000jc000317.
King, J.C., Anderson, P.S., Vaughan, D.G., Mann, G.W., Mobbs, S.D., Vosper, S.B., 2004. Wind-borne redistribution of snow across an Antarctic ice rise. J. Geophys. Res.-Atmos. 109 (D11), D11104. http://dx.doi.org/10.1029/2003jd004361.
Kingslake, J., Hindmarsh, R.C.A., Aðalgeirsdóttir, G., Conway, H., Corr, H.F.J., Gillet-Chaulet, F., Martín, C., King, E.C., Mulvaney, R., Pritchard, H.D., 2014. Full-depth englacial vertical ice sheet velocities measured using phase-sensitive radar. J. Geophys. Res. Earth Surf. 119 (12), 2604–2618. http://dx.doi.org/10.1002/2014jf003275.
Kulessa, B., Jansen, D., Luckman, A.J., King, E.C., Sammonds, P.R., 2014. Marine ice regulates the future stability of a large Antarctic ice shelf. Nat. Commun. 5, 3707. http://dx.doi.org/10.1038/ncomms4707.
Lange, M.A., MacAyeal, D.R., 1986. Numerical models of the Filchner–Ronne ice shelf: An assessment of reinterpreted ice thickness distributions. J. Geophys. Res. Solid Earth Planets 91 (B10), 457–462. http://dx.doi.org/10.1029/JB091iB10p10457.
Lenaerts, J.T.M., van den Broeke, M.R., 2012. Modeling drifting snow in Antarctica with a regional climate model: 2. Results. J. Geophys. Res.-Atmos. 117 (D5), D05109. http://dx.doi.org/10.1029/2010jd015419.
Lenaerts, J.T.M., Brown, J., Van Den Broeke, M.R., Matsuoka, K., Drews, R., Callens, D., Philippe, M., Gorodetskaya, I.V., Van Meijgaard, E., Reijmer, C.H., Pattyn, F., Van Lipzig, N.P.M., 2014. High variability of climate and surface mass balance induced by Antarctic ice rises. J. Glaciol. 60 (224), 1101–1110. http://dx.doi.org/10.3189/2014JoG14J040.
Lenaerts, J.T.M., van den Broeke, M.R., van de Berg, W.J., van Meijgaard, E., Kuipers Munneke, P., 2012. A new, high-resolution surface mass balance map of Antarctica

(1979–2010) based on regional atmospheric climate modeling. Geophys. Res. Lett. 39 (4), L04501. http://dx.doi.org/10.1029/2011gl050713.
Limbert, D.W., 1964. The absolute and relative movement, and regime of the Brunt Ice Shelf near Halley Bay. Brit. Antarc. Surv. Bull. 3, 1–11.
MacAyeal, D.R., Bindschadler, R.A., Shabtaie, S., Stephenson, S., Bentley, C.R., 1987. Force, mass, and energy budgets of the Crary Ice Rise complex, Antarctica. J. Glaciol. 33 (114), 218–230.
MacGregor, J.A., Winebrenner, D.P., Conway, H., Matsuoka, K., Mayewski, P.A., Clow, G.D., 2007. Modeling englacial radar attenuation at Siple Dome, West Antarctica, using ice chemistry and temperature data. J. Geophys. Res. Earth Surf. 112 (F3), F03008. http://dx.doi.org/10.1029/2006JF000717.
Mackintosh, A.N., Verleyen, E., O'Brien, P.E., White, D.A., Jones, R.S., McKay, R., Dunbar, R., Gore, D.B., Fink, D., Post, A.L., Miura, H., Leventer, A., Goodwin, I., Hodgson, D.A., Lilly, K., Crosta, X., Golledge, N.R., Wagner, B., Berg, S., van Ommen, T., Zwartz, D., Roberts, S.J., Vyverman, W., Masse, G., 2013. Retreat history of the East Antarctic Ice Sheet since the Last Glacial Maximum. Quat. Sci. Rev. 100, 10–30. http://dx.doi.org/10.1016/j.quascirev.2013.07.024.
Makinson, K., Nicholls, K.W., 1999. Modeling tidal currents beneath Filchner–Ronne Ice Shelf and on the adjacent continental shelf: their effect on mixing and transport. J. Geophys. Res. Oceans 104 (C6), 13449–13465. http://dx.doi.org/10.1029/1999jc900008.
Makinson, K., Holland, P.R., Jenkins, A., Nicholls, K.W., Holland, D.M., 2010. Influence of tides on melting and freezing beneath Filchner-Ronne Ice Shelf Antartica. Geophys. Res. Lett. 38 (6), L06601. http://dx.doi.org/10.1029/2010gl046462.
Martin, C., Gudmundsson, G.H., 2012. Effects of nonlinear rheology, temperature and anisotropy on the relationship between age and depth at ice divides. Cryosphere 6 (5), 1221–1229. http://dx.doi.org/10.5194/tc-6-1221-2012.
Martin, C., Gudmundsson, G.H., King, E.C., 2014. Modelling of Kealey Ice Rise, Antarctica, reveals stable ice-flow conditions in East Ellsworth Land over millennia. J. Glaciol. 60 (219), 139–146. http://dx.doi.org/10.3189/2014JoG13J089.
Martin, C., Gudmundsson, G.H., Pritchard, H.D., Gagliardini, O., 2009a. On the effects of anisotropic rheology on ice flow, internal structure, and the age-depth relationship at ice divides. J. Geophys. Res. Earth Surf. 114 (F4), F04001. http://dx.doi.org/10.1029/2008jf001204.
Martin, C., Hindmarsh, R.C.A., Navarro, F.J., 2009b. On the effects of divide migration, along-ridge flow, and basal sliding on isochrones near an ice divide. J. Geophys. Res. Oceans 114 (F2), F02006. http://dx.doi.org/10.1029/2008jf001025.
Martin, C., Hindmarsh, R.C.A., Navarro, F.J., 2006. Dating ice flow change near the flow divide at Roosevelt Island, Antarctica, by using a thermomechanical model to predict radar stratigraphy. J. Geophys. Res. Earth Surf. 111 (F1), F01011. http://dx.doi.org/10.1029/2005jf000326.
Martin, P.J., 1976. Ridges on Antarctic ice rises. J. Glaciol. 17 (75), 141–144.
Martin, P.J., Sanderson, T.J.O., 1980. Morphology and dynamics of ice rises. J. Glaciol. 25 (91), 33–45.
Massom, R.A., Giles, A.B., Fricker, H.A., Warner, R.C., Legresy, B., Hyland, G., Young, N., Fraser, A.D., 2010. Examining the interaction between multi-year landfast sea ice and the Mertz Glacier Tongue, East Antarctica: Another factor in ice sheet stability? J. Geophys. Res. Oceans 115 (C12), C12027. http://dx.doi.org/10.1029/2009jc006083.
Matsuoka, K., Pattyn, F., Callens, D., Conway, H., 2012. Radar characterization of the basal interface across the grounding zone of an ice-rise promontory in East Antarctica. Ann. Glaciol. 53 (60), 29–36. http://dx.doi.org/10.3189/2012aog60a106.
Miles, B.W.J., Stokes, C.R., Vieli, A., Cox, N.J., 2013. Rapid, climate-driven changes in outlet glaciers on the Pacific coast of East Antarctica. Nature 500 (7464), 563–566. http://dx.doi.org/10.1038/nature12382.
Morgan, V.I., Wookey, C.W., Li, J., vanOmmen, T.D., Skinner, W., Fitzpatrick, M.F., 1997. Site information and initial results from deep ice drilling on Law Dome, Antarctica. J. Glaciol. 43 (143), 3–10.
Mulvaney, R., Alemany, O., Possenti, P., 2007. The Berkner Island (Antarctica) ice-core drilling project. Ann. Glaciol. 47 (1), 115–124. http://dx.doi.org/10.3189/172756407786857758.
Mulvaney, R., Triest, J., Alemany, O., 2014. The James Ross Island and the Fletcher Promontory ice-core drilling projects. Ann. Glaciol. 55 (68), 179–188. http://dx.doi.org/10.3189/2014AoG68A044.
Naik, S.S., Thamban, M., Laluraj, C.M., Redkar, B.L., Chaturvedi, A., 2010. A century of climate variability in central Dronning Maud Land, East Antarctica, and its relation to Southern Annular Mode and El Nino–Southern Oscillation. J. Geophys. Res.-Atmos. 115 (D16), D16102. http://dx.doi.org/10.1029/2009jd013268.
Nereson, N.A., Raymond, C.F., 2001. The elevation history of ice streams and the spatial accumulation pattern along the Siple Coast of West Antarctica inferred from ground-based radar data from three inter-ice-stream ridges. J. Glaciol. 47 (157), 303–313. http://dx.doi.org/10.3189/172756501781832197.
Nereson, N.A., Waddington, E.D., 2002. Isochrones and isotherms beneath migrating ice divides. J. Glaciol. 48 (160), 95–108. http://dx.doi.org/10.3189/172756502781831647.
Nereson, N.A., Hindmarsh, R.C.A., Raymond, C.F., 1998a. Sensitivity of the divide position at Siple Dome, West Antarctica, to boundary forcing. Ann. Glaciol. 27, 207–214.
Nereson, N.A., Raymond, C.F., Jacobel, R.W., Waddington, E.D., 2000. The accumulation pattern across Siple Dome, West Antarctica, inferred from radar-detected internal layers. J. Glaciol. 46 (152), 75–87. http://dx.doi.org/10.3189/172756500781833449.
Nereson, N.A., Raymond, C.F., Waddington, E.D., Jacobel, R.W., 1998b. Migration of the Siple Dome ice divide, West Antarctica. J. Glaciol. 44 (148), 643–652.
Neumann, T.A., Conway, H., Price, P.B., Waddington, E.D., Catania, G., Morse, D.L., 2008. Holocene accumulation and ice-sheet dynamics in central West Antarctica. J. Geophys. Res. 113 (F2), F02018. http://dx.doi.org/10.1029/2007jf000764.
Nicholls, K.W., Osterhus, S., Makinson, K., Gammelsrod, T., Fahrbach, E., 2009. Ice–ocean processes over the continental shelf of the Southern Weddell Sea, Antarctica: A review. Rev. Geophys. 47 (3), RG3003. http://dx.doi.org/10.1029/2007rg000250.
Nicholls, K.W., Osterhus, S., Makinson, K., Johnson, M.R., 2001. Oceanographic conditions south of Berkner Island, beneath Filchner–Ronne Ice Shelf, Antarctica. J. Geophys. Res. Oceans 106 (C6), 11481–11492. http://dx.doi.org/10.1029/2000jc000350.
Nøst, O.A., Biuw, M., Tverberg, V., Lydersen, C., Hattermann, T., Zhou, Q., Smedsrud, L.H., Kovacs, K.M., 2011. Eddy overturning of the Antarctic Slope Front controls glacial melting in the Eastern Weddell Sea. J. Geophys. Res. Oceans 116 (C11), C11014. http://dx.doi.org/10.1029/2011jc006965.
Padman, L., Erofeeva, S., Joughin, I., 2003. Tides of the Ross Sea and Ross Ice Shelf cavity. Antarct. Sci. 15 (1), 31–40. http://dx.doi.org/10.1017/s0954102003001032.
Parrenin, F., Hindmarsh, R., 2007. Influence of a non-uniform velocity field on isochrone geometry along a steady flowline of an ice sheet. J. Glaciol. 53 (183), 612–622. http://dx.doi.org/10.3189/002214307784409298.
Pattyn, F., 2010. Antarctic subglacial conditions inferred from a hybrid ice sheet/ice stream model. Earth Planet. Sci. Lett. 295 (3–4), 451–461. http://dx.doi.org/10.1016/j.epsl.2010.04.025.
Pattyn, F., Matsuoka, K., Callens, D., Conway, H., Depoorter, M., Docquier, D., Hubbard, B., Samyn, D., Tison, J.L., 2012a. Melting and refreezing beneath Roi Baudouin Ice Shelf (East Antarctica) inferred from radar, GPS, and ice core data. J. Geophys. Res. 117 (F4), F04008. http://dx.doi.org/10.1029/2011jf002154.
Pattyn, F., Schoof, C., Perichon, L., Hindmarsh, R.C.A., Bueler, E., de Fleurian, B., Durand, G., Gagliardini, O., Gladstone, R., Goldberg, D., Gudmundsson, G.H., Huybrechts, P., Lee, V., Nick, F.M., Payne, A.J., Pollard, D., Rybak, O., Saito, F., Vieli, A., 2012b. Results of the Marine Ice Sheet Model Intercomparison Project, MISMIP. Cryosphere 6 (3), 573–588. http://dx.doi.org/10.5194/tc-6-573-2012.
Pettit, E.C., Jacobson, H.P., Waddington, E.D., 2003. Effects of basal sliding on isochrones and flow near an ice divide. Ann. Glaciol. 37 (1), 370–376. http://dx.doi.org/10.3189/172756403781815997.
Pettit, E.C., Thorsteinsson, T., Jacobson, H.P., Waddington, E.D., 2007. The role of crystal fabric in flow near an ice divide. J. Glaciol. 53 (181), 277–288. http://dx.doi.org/10.3189/172756507782202766.
Pettit, E.C., Waddington, E.D., Harrison, W.D., Thorsteinsson, T., Elsberg, D., Morack, J., Zumberge, M.A., 2011. The crossover stress, anisotropy and the ice flow law at Siple Dome, West Antarctica. J. Glaciol. 57 (201), 39–52. http://dx.doi.org/10.3189/002214311795306619.
Petty, A.A., Feltham, D.L., Holland, P.R., 2013. Impact of atmospheric forcing on Antarctic continental shelf water masses. J. Phys. Oceanogr. 43 (5), 920–940. http://dx.doi.org/10.1175/jpo-d-12-0172.1.
Pollard, D., DeConto, R.M., 2009. Modelling West Antarctic ice sheet growth and collapse through the past five million years. Nature 458 (7236), 329–332. http://dx.doi.org/10.1038/nature07809.
Pollard, D., DeConto, R.M., 2012. Description of a hybrid ice sheet-shelf model, and application to Antarctica. Geosci. Model Dev. 5 (5), 1273–1295. http://dx.doi.org/10.5194/gmd-5-1273-2012.
Price, S.F., Conway, H., Waddington, E.D., 2007. Evidence for late Pleistocene thinning of Siple Dome, West Antarctica. J. Geophys. Res. Earth Surf. 112 (F3), F03021. http://dx.doi.org/10.1029/2006jf000725.
Pritchard, H.D., Ligtenberg, S.R.M., Fricker, H.A., Vaughan, D.G., van den Broeke, M.R., Padman, L., 2012. Antarctic ice-sheet loss driven by basal melting of ice shelves. Nature 484 (7395), 502–505. http://dx.doi.org/10.1038/nature10968.
Raymond, C.F., 1983. Deformation in the vicinity of ice divides. J. Glaciol. 29 (103), 357–373.
Raymond, C.F., Nereson, N.A., Conway, H., 1995. Geometry and stratigraphy of Siple Dome, Antarctica. Antarct. J. US 30 (5), 91–93.
Rex, R.W., Margolis, S.V., Murray, B., 1970. Possible interglacial dune sands from 300 meters water depth in Weddell Sea, Antarctica. Geol. Soc. Am. Bull. 81 (11), 3465–3472. http://dx.doi.org/10.1130/0016-7606(1970)81[3465:pidsfm]2.0.co;2.
Rignot, E., 2002. Ice-shelf changes in Pine Island Bay, Antarctica, 1947–2000. J. Glaciol. 48 (161), 247–256. http://dx.doi.org/10.3189/172756502781831386.
Rignot, E., 2008. Changes in West Antarctic ice stream dynamics observed with ALOS PALSAR data. Geophys. Res. Lett. 35 (12), L12505. http://dx.doi.org/10.1029/2008gl033365.
Rignot, E., Jacobs, S., Mouginot, J., Scheuchl, B., 2013. Ice-shelf melting around Antarctica. Science 341 (6143), 266–270. http://dx.doi.org/10.1126/science.1235798.
Rignot, E., Mouginot, J., Morlighem, M., Seroussi, H., Scheuchl, B., 2014. Widespread, rapid grounding line retreat of Pine Island, Thwaites, Smith, and Kohler glaciers, West Antarctica, from 1992 to 2011. Geophys. Res. Lett. 41 (10), 3502–3509. http://dx.doi.org/10.1002/2014gl060140.
Rignot, E., Mouginot, J., Scheuchl, B., 2011a. Ice Flow of the Antarctic Ice Sheet. Science 333 (6048), 1427–1430. http://dx.doi.org/10.1126/science.1208336.
Rignot, E., Mouginot, J., Scheuchl, B., 2011b. Antarctic grounding line mapping from differential satellite radar interferometry. Geophys. Res. Lett. 38, L10504. http://dx.doi.org/10.1029/2011gl047109.
Roberts, J.L., Moy, A.D., van Ommen, T.D., Curran, M.A.J., Worby, A.P., Goodwin, I.D., Inoue, M., 2013. Borehole temperatures reveal a changed energy budget at Mill Island, East Antarctica, over recent decades. Cryosphere 7 (1), 263–273. http://dx.doi.org/10.5194/tc-7-263-2013.
Robin, G.D., 1953. Measurements of ice thickness in Dronning Maud Land, Antarctica. Nature 171 (4341), 55–58. http://dx.doi.org/10.1038/171055a0.
Scambos, T.A., Haran, T.M., Fahnestock, M.A., Painter, T.H., Bohlander, J., 2007. MODIS-based Mosaic of Antarctica (MOA) data sets: Continent-wide surface morphology and snow grain size. Remote Sens. Environ. 111 (2–3), 242–257. http://dx.doi.org/10.1016/j.rse.2006.12.020.
Schmeltz, M., Rignot, E., Macayeal, D.R., 2001. Ephemeral grounding as a signal of ice-shelf change. J. Glaciol. 47 (156), 71–77. http://dx.doi.org/10.3189/172756501781832502.

Schoof, C., 2007. Ice sheet grounding line dynamics: Steady states, stability, and hysteresis. J. Geophys. Res. Earth Surf. 112 (F3), F03S28. http://dx.doi.org/10.1029/2006jf000664.
Schoof, C., Hindmarsh, R.C.A., 2010. Thin-film flows with wall slip: an asymptotic analysis of higher order glacier flow models. Q. J. Mech. Appl. Math. 63 (1), 73–114. http://dx.doi.org/10.1093/qjmam/hbp025.
Scientific Committee on Antarctic Research, 2012. Antarctic Digital Database Version 6.0.
Sergienko, O.V., 2013. Basal channels on ice shelves. J. Geophys. Res. Earth Surf. 118 (3), 1342–1355. http://dx.doi.org/10.1002/jgrf.20105.
Shipp, S., Anderson, J., Domack, E., 1999. Late Pleistocene–Holocene retreat of the West Antarctic Ice-Sheet system in the Ross Sea: Part 1 — Geophysical results. Geol. Soc. Am. Bull. 111 (10), 1486–1516. http://dx.doi.org/10.1130/0016-7606(1999)1117606(1999)1111486:LPHROT>2.3.CO;2.
Siegert, M., Ross, N., Corr, H., Kingslake, J., Hindmarsh, R., 2013. Late Holocene ice-flow reconfiguration in the Weddell Sea sector of West Antarctica. Quat. Sci. Rev. 78, 98–107. http://dx.doi.org/10.1016/j.quascirev.2013.08.003.
Sinclair, K.E., Bertler, N.A.N., Bowen, M.M., Arrigo, K.R., 2014. Twentieth century sea-ice trends in the Ross Sea from a high-resolution, coastal ice-core record. Geophys. Res. Lett. 41 (10), 3510–3516. http://dx.doi.org/10.1002/2014gl059821.
Smith, A.M., 1986. Ice rumples on Ronne Ice Shelf, Antarctica. Brit. Antarc. Surv. Bull. 72, 47–52.
Smith, A.M., 1991. The use of tiltmeters to study the dynamics of Antarctic ice-shelf grounding lines. J. Glaciol. 37 (125), 51–58.
Stewart, A.L., Thompson, A.F., 2015. Eddy-mediated transport of warm Circumpolar Deep Water across the Antarctic Shelf Break. Geophys. Res. Lett. 42 (2), 432–440. http://dx.doi.org/10.1002/2014gl062281.
Stone, J.O., Balco, G.A., Sugden, D.E., Caffee, M.W., Sass, L.C., Cowdery, S.G., Siddoway, C., 2003. Holocene deglaciation of Marie Byrd Land, West Antarctica. Science 299 (5603), 99–102. http://dx.doi.org/10.1126/science.1077998.
Swithinbank, C., 1977. Glaciological research in the Antarctic Peninsula. Philos. Trans. R. Soc. Lond. B 279 (963), 161–183. http://dx.doi.org/10.1098/rstb.1977.0080.
Tamura, T., Ohshima, K.I., Nihashi, S., 2008. Mapping of sea ice production for Antarctic coastal polynyas. Geophys. Res. Lett. 35 (7), L07606. http://dx.doi.org/10.1029/2007gl032903.
Taylor, K.C., Alley, R.B., Meese, D.A., Spencer, M.K., Brook, E.J., Dunbar, N.W., Finkel, R.C., Gow, A.J., Kurbatov, A.V., Lamorey, G.W., Mayewski, P.A., Meyerson, E.A., Nishiizumi, K., Zielinski, G.A., 2004. Dating the Siple Dome (Antarctica) ice core by manual and computer interpretation of annual layering. J. Glaciol. 50 (170), 453–461. http://dx.doi.org/10.3189/172756504781829864.
Thoma, M., Jenkins, A., Holland, D., Jacobs, S., 2008. Modelling Circumpolar Deep Water intrusions on the Amundsen Sea continental shelf, Antarctica. Geophys. Res. Lett. 35 (18), L18602. http://dx.doi.org/10.1029/2008GL034939.
Thomas, E.R., Marshall, G.J., McConnell, J.R., 2008. A doubling in snow accumulation in the western Antarctic Peninsula since 1850. Geophys. Res. Lett. 35 (1), L01706. http://dx.doi.org/10.1029/2007gl032529.
Thomas, R.H., 1971. Flow law for Antarctic ice shelves. Nat. Phys. Sci. 232 (30), 85–87. http://dx.doi.org/10.1038/physci232085a0.
Thomas, R.H., 1973a. The creep of ice shelves: theory. J. Glaciol. 12 (64), 45–53.
Thomas, R.H., 1973b. The creep of ice shelves: interpretation of observed behavior. J. Glaciol. 12 (64), 55–70.
Thomas, R.H., 1979. Ice shelves: a review. J. Glaciol. 24 (90), 167–177.
Thomas, R.H., MacAyeal, D.R., 1982. Derived characteristics of the Ross Ice Shelf, Antarctica. J. Glaciol. 28 (100), 397–412.
Tinto, K.J., Bell, R.E., 2011. Progressive unpinning of Thwaites Glacier from newly identified offshore ridge: Constraints from aerogravity. Geophys. Res. Lett. 38 (20), L20503. http://dx.doi.org/10.1029/2011gl049026.
Van de Berg, W.J., van den Broeke, M.R., Reijmer, C.H., van Meijgaard, E., 2006. Reassessment of the Antarctic surface mass balance using calibrated output of a regional atmospheric climate model. J. Geophys. Res.-Atmos. 111 (D11), D11104. http://dx.doi.org/10.1029/2005JD006495.
Van Lipzig, N.P.M., Turner, J., Colwell, S.R., Van Den Broeke, M.R., 2004. The near-surface wind field over the Antarctic continent. Int. J. Climatol. 24 (15), 1973–1982. http://dx.doi.org/10.1002/joc.1090.
Van Ommen, T.D., Morgan, V., Curran, M.A.J., 2004. Deglacial and Holocene changes in accumulation at Law Dome, East Antarctica. Ann. Glaciol. 39 (1), 359–365. http://dx.doi.org/10.3189/172756404781814221.
Vaughan, D.G., Anderson, P.S., King, J.C., Mann, G.W., Mobbs, S.D., Ladkin, R.S., 2004. Imaging of firn isochrones across an Antarctic ice rise and implications for patterns of snow accumulation rate. J. Glaciol. 50 (170), 413–418. http://dx.doi.org/10.3189/172756504781829882.
Vaughan, D.G., Corr, H.F.J., Doake, C.S.M., Waddington, E.D., 1999. Distortion of isochronous layers in ice revealed by ground-penetrating radar. Nature 398 (6725), 323–326. http://dx.doi.org/10.1038/18653.
Vaughan, D.G., Marshall, G.J., Connolley, W.M., Parkinson, C., Mulvaney, R., Hodgson, D.A., King, J.C., Pudsey, C.J., Turner, J., 2003. Recent rapid regional climate warming on the Antarctic Peninsula. Clim. Chang. 60 (3), 243–274. http://dx.doi.org/10.1023/a:1026021217991.
Waddington, E.D., Conway, H., Steig, E.J., Alley, R.B., Brook, E.J., Taylor, K.C., White, J.W.C., 2005. Decoding the dipstick: Thickness of Siple Dome, West Antarctica, at the Last Glacial Maximum. Geology 33 (4), 281–284. http://dx.doi.org/10.1130/g21165.1.
Waddington, E.D., Neumann, T.A., Koutnik, M.R., Marshall, H.P., Morse, D.L., 2007. Inference of accumulation-rate patterns from deep layers in glaciers and ice sheets. J. Glaciol. 53 (183), 694–712. http://dx.doi.org/10.3189/002214307784409351.
Wang, W.L., Warner, R.C., Budd, W.F., 2002. Ice-flow properties at Dome Summit South, Law Dome, East Antarctica. Ann. Glaciol. 35 (1), 567–573. http://dx.doi.org/10.3189/172756402781816924.
Weber, M.E., Clark, P.U., Kuhn, G., Timmermann, A., Sprenk, D., Gladstone, R., Zhang, X., Lohmann, G., Menviel, L., Chikamoto, M.O., Friedrich, T., Ohlwein, C., 2014. Millennial-scale variability in Antarctic ice-sheet discharge during the last deglaciation. Nature 510 (7503), 134–138. http://dx.doi.org/10.1038/nature13397.
Weertman, J., 1974. Stability of the junction of an ice sheet and an ice shelf. J. Glaciol. 13 (67), 3–11.
Whillans, I.M., 1973. State of equilibrium of the West Antarctic inland ice sheet. Science 182 (4111), 476–479. http://dx.doi.org/10.1126/science.182.4111.476.
Whitehouse, P.L., Bentley, M.J., Milne, G.A., King, M.A., Thomas, I.D., 2012. A new glacial isostatic adjustment model for Antarctica: calibrated and tested using observations of relative sea-level change and present-day uplift rates. Geophys. J. Int. 190 (3), 1464–1482. http://dx.doi.org/10.1111/j.1365-246X.2012.05557.x.
Wilson, D.S., Luyendyk, B.P., 2006. Bedrock platforms within the Ross Embayment, West Antarctica: Hypotheses for ice sheet history, wave erosion, Cenozoic extension, and thermal subsidence. Geochem. Geophys. Geosyst. 7 (12), Q12011. http://dx.doi.org/10.1029/2006gc001294.
Zhou, Q., Hattermann, T., Nøst, O.A., Biuw, M., Kovacs, K.M., Lydersen, C., 2014. Wind-driven spreading of fresh surface water beneath ice shelves in the Eastern Weddell Sea. J. Geophys. Res. Oceans 119 (6), 3818–3833. http://dx.doi.org/10.1002/2013jc009556.